Positive cerium anomaly in the Doushantuo cap carbonates from Yangtze platform, South China: Implication for intermediate manganous conditions in the water column in the aftermath of Marinoan glaciation

He-Pin Wu[a], Shao-Yong Jiang[a,b,*], Martin Palmer[c], Haizhen Wei[a], Jing-Hong Yang[a]

[a]*State Key Laboratory for Mineral Deposits Research, Department of Earth Sciences, Nanjing University, Nanjing 210023, China*

[b]*State Key Laboratory of Geological Processes and Mineral Resources, Collaborative Innovation Center for Exploration of Strategic Mineral Resources, Faculty of Earth Resources, China University of Geosciences, Wuhan 43074, China*

[c]*National Oceanography Centre, School of Ocean and Earth Science, University of Southampton, Southampton SO14 3ZH, UK*

*Corresponding authors: shyjiang@cug.edu.cn (S.-Y. Jiang)

ABSTRACT

Oxygenation exerts an important control on the emergence and diversification of metazoans in the aftermath of Marinoan glaciation. However, the relationship between oceanic dissolved O_2 (DO) level and early metazoan evolution remains equivocal. In order to provide a precise temporal and spatial reconstruction of the redox conditions for this critical time period, we studied cap carbonates across a shelf to basin transect in three localities in the Three Gorges area, Yangtze platform, South China. Trace and rare earth elements are determined by sequential extraction of carbonate fraction to present pristine temporal seawater signal. The dolomites in the Member II of Doushantuo Formation just above the cap carbonates show negative Ce anomaly. In contrast, no Ce anomalies are observed in the lower units of cap carbonates. A compelling positive Ce anomaly (Ce/Ce^*>1.3) has been observed in the demise of cap carbonate deposition in all studied sections. These positive Ce anomalies accompany with high Mn/Fe ratios and insignificant MREE anomalies, suggesting a Fe-Mn-(oxyhydro) oxide co-participation during cap carbonate deposition. It is suggested that positive Ce anomalies may result from the reductive dissolution of Ce enriched Mn-(oxyhydro) oxides across a Mn(IV)/Mn(II) redoxcline, in a distinct manganous wedge sandwiched between well oxygenated and anoxic ferruginous deep water column. The highlighted wedge may represent a low oxygen condition with roughly 10 μM DO in comparison with the >90 μM DO of the oxic setting, as well as 0 μM DO of the anoxic condition. The presence of positive Ce anomalies in the uppermost part of cap carbonates may provide a novel insight for indicating intermediate manganous conditions in the water column, and further constraining the redox structure of terminal Ediacaran cap carbonate deposition. Early Ediacaran metazoans were likely restricted to fully oxygenated conditions, and were absent where conditions were manganous or ferruginous.

Keywords: Marinoan cap carbonates; positive Ce anomaly; Mn-(oxyhydr) oxides; Three Gorges area; Yangtze platform

1. Introduction

After the Marinoan meltdown, the Ediacaran period witnesses dramatic diversification of multicellular life as well as a remarkable change of global climate and geochemical cycle (Kirschvink, 1992; Hoffman et al., 1998; Higgins and Schrag, 2003; Caxito et al., 2012). The occurrence of widespread carbonate deposition that immediately overlie above the diamictites, known as cap carbonate, commonly preserve striking features of the climate and environment shifts at the termination of the glaciation (Hoffman et al., 1998; Shields, 2005; Bechstädt et al., 2018; Caxito et al., 2018). The cap carbonates usually exhibit negative $\delta^{13}C$ anomaly (Jiang et al., 2003; Rose and Maloof, 2010; Zhu et al., 2013) and unique sedimentary structures and textures, such as the pseudo-tepees, tube structures, and aragonite fans (Kennedy et al., 1998; James et al., 2001; Lorentz et al., 2004). The depositional time interval of several meters thick cap carbonates is not exceeding than 1 Ma (Hyde et al., 2000; Higgins and Schrag, 2003; Font et al., 2010), thus the high-rate depositional water property may thus provide a vital insight into revealing palaeoceangraphic environmental evolution.

The distribution patterns of rare earth elements and yttrium (REYs) are frequently used as proxies for ancient seawater chemistry. Studies on various well-preserved sedimentary rocks precipitated in paleo seawater have been previously carried out, including biogenic apatite (conodonts, fish scales and otoliths, and vertebrate bones) (Arslan and Paulson, 2003; Lécuyer et al., 2003; Song et al., 2012; Chen et al., 2015), skeletal carbonate (Webb and Kamber, 2000; Nothdurft et al., 2004; Wyndham et al., 2004) and hydrogenous sediments (chert, phosphorite and carbonate) (Murray et al., 1991; Mazumdar et al., 2003; Shields and Webb, 2004; Ling et al., 2013; Xin et al., 2015). In the aspect of carbonate chemistry, REYs can substitute for the calcium ion into the lattice structure of authigenic phases without fractionation during diagenesis, including even dolomitization and dissolution and re-adsorption processes (Reynard et al., 1999; Webb et al., 2009; Guido et al., 2011; Sarangia et al., 2017). Recently, studies on cap carbonates have been conducted to reflect temporal seawater signals (Font et al., 2006; Huang et al., 2009; Zhao et al., 2009; Yan et al., 2010; Huang et al., 2011; Meyer et al., 2012; Tian et al., 2014; Wang et al., 2014; Hu et al., 2016; Caxito et al., 2018). Previous workers draw their attention to various deposition fluids and material sources with REY analysis. For example, Huang et al. (2011) outlined a hydrothermal origin of redox-sensitive trace elements for the cap carbonates. Zhao et al. (2018) also indentified different contribution of high-temperature hydrothermal fluids to the cap carbonates from South China. Several studies also claimed that local deglacial meltwater interfused with seawater as precipitation water for the cap carbonates that deposited in a weak oxic condition (Zhao et al., 2009; Yan et al., 2010; Caxito et al., 2018).

The behavior of cerium in sweater has been widely interpreted regarding water mass redox conditions for marine sediments. It is noteworthy that positive Ce anomaly was previously reported in some of the cap carbonate samples (Ling et al., 2013; Wang et al., 2014; Hu et al., 2016). However, these authors did not give a meaningful interpretation for the positive Ce anomaly. This paper here devotes to account for the reason of positive Ce anomalies found in the top of cap carbonates in several sections from deep to shallow water on the Yangtze platform, and further decodes the variation of redoxcline interfaces and the palaeoenvironmental implications.

2. Geological setting

Doushantuo Formation is one of the world's best-preserved Neoproterozoic Ediacaran carbonate sequences that deposited on the passive marginal sea basin of the Yangtze platform and developed in the aftermath of the Marinoan glaciation (e.g., Wang and Li, 2003; Jiang et al., 2006; Vernhet et al., 2006) (Fig.1a, b). The Doushantuo Formation has been well defined stratigraphically and ecologically (Zhu et al., 2003; Yuan et al., 2011; Zhu et al., 2013), it is typically divided into four lithological members and hosting abundant three-dimensionally preserved eukaryotes. The cap carbonate member (which usually just several meters in thickness) in the base of Doushantuo Formation rests disconformably overlain by the Nantuo diamictite Formation.

The age of the onset of cap carbonate deposition has been constrained from zircon U-Pb methods, including an age of 628.3±5.8 Ma (Yin et al., 2005) or 621±7 Ma (Zhang et al., 2005) obtained from the volcanic ash layers within the upper cap carbonates. Condon et al. (2005) has constrained the age to 635.2±0.6 Ma from the cap carbonates of the Doushantuo Formation in Wuhe-Gaojiaxi section in the Three Gorges area. These results are in consistent with the age of 635.5±0.5 Ma reported for the Ghaub Formation in Namibia (Hoffmann et al., 2004). Therefore, the beginning of cap carbonate precipitation is considered at ca. 635 Ma, as the termination of Marinoan glaciation.

Three sections of cap carbonates (Huajipo, Wuhe and Jiulongwan) were examined in this study, which cover a range of paleo-facies from the shallow intra-shelf to the inner basin (Fig. 1c). Both Huajipo section (30˚46′55.6″N, 111˚01′08.2″E) and Wuhe section (30˚46′54.57″N, 111˚02′03.49″E) represent deposition in the shallow inner basin facies, whereas the Jiulongwan section (30˚48′14.5″N, 111˚03′20.1″E) represents an intra-shelf facies. They are all located at the southern limb of the Huangling Granite Anticline near the Sandouping Village and within the distance of no more than 5 km. The three sections deposited in a locally restricted palaeooceanic setting and show thickness of several meters with three lithological units of CA1, CA2 and CA3 (Jiang et al., 2003) (Fig. 2). The basal CA1 unit consists of microcrystalline dolomite that is commonly brecciated and contains cavities lined by multiple generations of fringing cement. The middle layer (CA2) is characterized by laminated dolomicrites with "tepee-like" structures that disrupt laminations at its base. The upper layer (CA3) consists of thinly laminated, silty, limestones and dolomicrites.

3. Samples and analytical methods

In this study, we selected 63 samples for trace and rare earth elements and carbon-oxygen isotope measurements from the three cap carbonates sections.

A critical issue in using trace and rare earth elements of carbonate rocks for indicating water mass redox conditions is the potential overprinting of the pristine seawater signal via alteration. To obtain high-quality samples in which original rare earth elements signals are well preserved, we firstly screened macroscopically in the field to choose samples without weathered surfaces, and then examined microscopically to avoid from feldspar-quartz veins and miarolitic structures. Fresh carbonate samples were then pulverized to powder by diamond tipped micro-drill (Proxxon, Germany) and further ground to 200 mesh with agata-pestle type grinding machine (Retsch, Germany).

Twenty milligramms of powder from each sample were used for $\delta^{13}C$ and $\delta^{18}O$ analysis. Dolomite samples were reacted with 100% H_3PO_4 at 50℃ for more than 24h in the laboratory of the Nanjing Institute of Geology and Palaeontology, Chinese Academy of Sciences. Prepared gas samples were analyzed for $\delta^{13}C$ and $\delta^{18}O$ using the Chinese national standard, an Ordovician carbonate from a site near Beijing (reference number GBW 04405: $\delta^{13}C = 0.57 \pm 0.03$ ‰ VPDB; $\delta^{18}O = -8.49 \pm 0.13$ ‰ VPDB). The analysis was carried out using a Finnegan MAT 253 mass spectrometer in the State Key Laboratory for Mineral Deposits Research, Nanjing University. The $\delta^{13}C$ precision was better than 0.15‰, and that of $\delta^{18}O$ was better than 0.1‰.

Previous methods applied for carbonate dissolution in trace and rare earth elements use varying acid types (Tessier et al., 1979; Shields et al., 1997; Nothdurft et al., 2004; Zhao et al., 2009) or varying acid strengths under different reaction temperature and dissolution of time (Bodin et al., 2007). The dissolution leaching procedures are carried out with single-step or partial dissolution methods (Zhao et al., 2009; Meyer et al., 2012; Zhang et al., 2015). Tostevin et al. (2016a) and Zhang et al. (2015) have systematically investigated the proposed dissolution methods with acetic acid in sequential leaching. They suggested that the REY patterns show similar trends with different acid strength during the second step, and the non-carbonate minerals such as terrestrial particulate matter, Fe-Mn-(oxyhydr) oxides, phosphates and organic matters that affect REY distribution patterns will be dissolved when excess acid is added. Dolomite samples do not need sequential leaching step due to the dissolving products show similar REE patterns as the first step do. Besides, nitric acid acts as an oxidizing acid will dissolve the organic matters in samples, to some extent. Therefore, considering the non-carbonate phases absorbed on the cap carbonates, we chose the 10% acetic acid (GR) to dissolve the dolomite phase to represent the palaeo seawater signature. The trace elements and REE analyses were undertaken at National Oceanography Centre (NOC), University of Southampton, United Kingdom. About 100 mg samples were leached in sealed polypropylene centrifuge tubes using 2 mL of 10% acetic acid (HAC). The partial solutions that completely reacted with acetic acid over 24 hours were ultrasonic stirred and centrifuged. The supernatant then transferred to clean Teflon bottles, and the residue were washed three times with Mill-Q water, centrifuged and transferred to the Teflon bottles. Then we added 6M HCl to the dried samples and diluted with Mill-Q to 10 mL as mother solutions. 0.5 mL mother solutions were then evaporated to dryness and added 3% HNO_3 with 5 ppb In and Re and 200 ppb Be to yield a 1,000-fold diluted solution. Analyses were carried out on an Inductively Coupled Plasma Mass Spectrometry (ICP-MS) (Thermo Finnigan, Bremen, Germany) with multi-standard elements calibration solution. For trace element analysis, spectral interferences from major elements Fe, Al, Ca, Mg were monitored and corrected as necessary using single-element standards. The analytical error was 0.5 to 3%

and the accuracy was 5%. The REE data are presented as Post-Archean Average Shale (PAAS)-normalized (McLennan, 1989; Pourmand et al., 2012) plots, and the Eu/Eu*, Ce/Ce* and MREE/MREE* are calculated from the PAAS-normalized values with published formulae (Lawrence et al., 2006; Ling et al., 2013; Chen et al., 2015):

$$MREE/MREE^* = \frac{2\times([Sm]_n+[Gd]_n+[Dy]_n+[Tb]_n)/4}{([La]_n+[\mathrm{Pr}]_n+[Nd]_n)/3+([Ho]_n+[Er]_n+[Tm]_n+[Yb]_n+[Lu]_n)/5} \quad (1)$$

$$Eu/Eu^* = Eu_n/(Sm_n^2\times Tb_n)^{1/3} \quad (2)$$

$$Ce/Ce^* = Ce_n/(\mathrm{Pr}_n^2/Nd_n) \quad (3)$$

These calculations will avoid the artificial exaggeration of La anomaly to Ce anomaly.

4. Results

4.1. Major and trace elements

The major and trace elemental data of carbonate samples from all studied sections are listed in Table 1. The $CaCO_3$ percentages of cap carbonates entirely are excess than 20%, and that of basin samples (Huajipo and Wuhe sections) is about 10% lower than intra-shelf ones (Jiulongwan section) (Table 1). Mg (wt.%) data present the relative lower data in intra-shelf samples (0.03-2.53%) than the basin samples (0.4-9.5%). Most carbonate components have low Al concentrations (<0.6 wt.%). Mn and Fe concentrations are relative high with thousands ppm. Ba concentrations show lower values in CA2 units (<100 ppm) compared with the basal and top units of cap carbonate, in where the values can reach to hundreds ppm. Strontium concentration display the similar rule as Ba does, ranging from 44 to 247 ppm. The basin samples have similar values of Pb and Cu concentrations and they all are below to 12 ppm. All studied sections have similar Sc and Co concentrations with several ppm in most.

4.2. Oxygen and carbon isotopic compositions

The $\delta^{18}O$ values of the cap carbonates are relatively invariant higher than -10‰. In contrast, the carbon isotope values ($\delta^{13}C$) of the cap carbonates are highly variable ranging from 0.4 to -22.5 ‰. The $\delta^{13}C$ data are in good agreement with literature data (Jiang et al., 2007; McFadden et al., 2008; Wang et al., 2008), showing a stage of constant $\delta^{13}C$ values around -5‰ before the extremely negative $\delta^{13}C$ values obtained from the end of cap carbonates, and return toward to above 3‰ in the overlying member II sediments (Table 1).

4.3. Rare earth elements and REY patterns

The rare earth element data and relative ratios from all studied sections are listed in Table 2. Detrital siliciclastic influenced samples may exhibit high ΣREE more than hundreds ppm. However, our ΣREE data all below 60 ppm, indicating a dominant hydrogenous sourced REE. The Y/Ho ratio shows a range from 36 to 53, which is similar to the seawater value (Fig. 2). Broadly speaking, Ce/Ce^* ratios of carbonates exhibit similar range from basin samples (0.90-1.64) to intra-shelf samples (0.86-1.34). No distinct Ce anomalies (Ce/Ce^* around 1.0) are detected during the CA1 and CA2 units of the three sections. The Member II of Jiulongwan and Huajipo section present negative Ce anomalies with ratios around 0.9. The most intriguing observation to emerge from the data is the positive Ce anomalies found in the top of CA3 units in all three sections (Fig. 2).

REY patterns of the three studied sections can be categorized as three lithological units (Fig. 3). In CA1 unit, the REY patterns of Jiulongwan and Huajipo sections are characterized by relative flat patterns but the Wuhe section shows a LREE-depleted pattern (Fig. 3a, d, g). The REY patterns in CA2 units display slight MREE-bulge pattern, samples in lower parts have obvious seawater signals with LREE-depleted and positive Y anomalies (Fig. 3b, e, h). The LREE-enriched REY patterns together with positive Y and La anomalies are shown for CA3 units (Fig. 3c, f, i). The positive Eu anomalies mixed with LREE-depleted patterns ($Pr_N/Yb_N<1.0$) may be considered as syn-hydrothermal fluids incorporated with seawater (Fig. 3).

5. Discussion

5.1. Fidelity of trace and rare earth elements

Deducing the properties of the precipitating waters and depositional environment using trace elements data needs firstly to confirm these elements originated from authigenic sediments as a prerequisite. There are generally four critical sources of contamination, including (1) detrital components effect, (2) diagenetic alteration effect, (3) submarine hydrothermal alteration and (4) instrumental measurement error (Tribovillard et al., 2006; Sarangia et al., 2017).

In the authigenic marine sediments, the existence of small amounts of detrital silicate minerals such as clay minerals, quartz and feldspar may affect the REEs signature of paleo seawater that recorded in the authigenic minerals. In this study, we use a 10% acetic acid dissolution protocol to avoid attack of the detrital silicate minerals in the samples. High field strength elements (e.g. Sc, Zr, Ti) are mainly derived from terrestrial products, so they are suitable to monitor the extent of terrestrial particulate matters contamination (Calvert and Pedersen, 1993; Böning et al., 2004; Schröder and Grotzinger, 2007). Using the acetic acid dissolution method, the mass percentage of $CaCO_3$, Sc/Ca and Al/Ca ratios in our studied cap carbonate samples show no correlation with Ce anomaly, indicating a negligible detrital contribution. To maximum exclude the detrital effects, criteria that Al/Ca < 8 ppm and $CaCO_3$ > 20% are followed to examine the carbonate Ce/Ce^* values (Fig. 4a-c). In order to evaluate the contamination from sulfides and oxides, the elements Pb and Cu can be used together with Y/Ho ratios (Wang et al., 2014). Our samples also show no correlations between Y/Ho and Pb/Ca or Cu/Ca, indicating the contamination by sulfides and oxides can be excluded (Fig. 4d,e). In spite of similar ionic radius, valence state and geochemical behaviors, Ho is scavenged from seawater twice as fast as Y because of differences in surface complexation ability (Liu and Byrne, 1995; Nozaki et al., 1997). Fractionation between Y and Ho during weathering and fluvial transport to the ocean appears to slightly affect the Y/Ho ratio of seawater, and the Ho reflects changes in near/far shore environments of deposition due to its property of tracking the connectivity of a water column to the open ocean (Johannesson et al., 2006; Nozaki et al., 1997). Y/Ho ratio thus can be considered as a good indicator to distinguish marine and non-marine deposition (Nothdurft et al., 2004). Modern seawater exhibits distinct positive Y anomaly, with values of 40-80 for open marine setting and 33-40 for near-shore or restricted basin setting

(Nozaki and Zhang, 1995; Bau et al., 1997). Therefore, in this study, we only use those samples with Y/Ho>36 as unaltered seawater REY signatures following the suggestion by Tostevin et al. (2016a) (Fig.4f).

The REY patterns of marine carbonates can also be modified by diagenetic alteration. Diagenetic fluids, such as burial fluids, meteoric fluids, hydrothermal fluids and/or dolomitization fluids, may all slightly affect REY signatures of sedimentary carbonates (Guido et al., 2011). Several previous works on Devonian limestones and Carboniferous marine limestones suggested that these samples still preserved their original REY signatures without contamination by mineralizing fluids or dolomitization events (Parekh et al., 1977; Banner et al., 1988; Nothdurft et al., 2004). To maximum eliminate the effect caused by diagenetic fluids, criteria including $\delta^{18}O$<-10‰, Mn/Sr> 2 and high Mn content are usually recognized as good indicators to avoid those carbonate samples with diagenetic alteration (Derry et al., 1994; Jacobsen and Kaufman, 1999). The $\delta^{18}O$ values of most cap carbonates samples are mostly ranged from -10‰ to 0‰ except some scatters pointed less than -10‰ (Fig. 5a, b). These scattered samples are mainly from the basal cap carbonates and the top layers above the cap carbonates. One alterative explanation for the low $\delta^{18}O$ values in the base cap carbonates may be attributed to their participation from glacial melting water mass (Zhao and Zheng, 2010), so these authors suggested that the isotopic values within the CA1 unit can be regarded as unaltered. Previously reported Mn/Sr ratios of early Cryogenian and Neoproterozoic cap carbonates are commonly high, and this has been attributed as the unusual coeval seawater chemistry in anoxic or suboxic depositional environments by many researchers (Yoshioka et al., 2003; Font et al., 2006; Hurtgen et al., 2006). Therefore, in this study we apply a Mn/Sr ratio of <62 as the cutoff value to exclude the samples with diagenetic alteration (Fig. 5b, c). Of note, there exists no correlation between the Ca normalization Mn and Fe concentrations and Ce anomaly (Fig. 5d, e), which also indicates a negligible diagenetic effect. A strong covariation would appear between Ce/Ce^{*} and Eu/Eu^{*} or Dy_N/Sm_N if the REY patterns of the cap carbonates experienced diverse degrees of diagenetic effect (Shields and Stille, 2001), but no obvious positive correlation between Ce/Ce^{*} and Eu/Eu^{*} or Dy_N/Sm_N occurs in the our studied samples from the three sections (Fig. 5f, h), which again suggest that the REY of the cap carbonates are unaffected by diagenetic alteration and therefore these data can be used as representations for original REY compositions that record the paleo seawater signatures.

The submarine hydrothermal process can also influence the trace and rare earth elements contents of marine sediments. Normally the hydrothermal fluids can provide abundant Ba, Sr, Pb, Zn and Mn to the sediments (Pujol et al., 2006). Moreover, the addition of abundant Fe and Mn from hydrothermal fluids may cause a partial change of redox state, resulting to some redox-sensitive element enrichments (Morford et al., 2001). The most prominent characteristics of submarine hydrothermal fluids are remarkable positive Eu anomaly and LREE enrichment (Michard and Albarede, 1986; Campbell et al., 1988; James et al., 1995). The Eu^{3+}/Eu^{2+} redox potential in waters mainly depends on temperature, pH and REE speciation (Bau, 1991). Some samples in the studied sections are excluded because of their abnormally high La_N/Yb_N (2.4) and Gd_N/Yb_N (2.57) ratios (Fig. 5i). Most samples display positive Eu anomaly, which may indicate an effect from syn-depositional hydrothermal fluids.

In the Eu measurement with ICP-MS, high content of Ba would influence Eu values, making false positive Eu anomalies (Jiang et al., 2007). In order to exclude this analytical effect, the crossplot of Eu/Eu* vs Ba/Nd is examined, and our studied samples show no correlation between them (R^2=0.063) (Fig. 5g), that is to say the positive Eu anomaly in the samples are not artificial but genuine result.

In summary, in this study we use the following criteria, including $\delta^{18}O$ < -10 ‰, Al/Ca < 8 ppm, $CaCO_3$ > 20%, Y/Ho > 36, Ba/Nd < 100 and Eu/Eu* < 2 to select the genuine data for the cap carbonate samples that may record the pristine paleo seawater signature. In Table 1 and 2, the asterisk-labeled samples are excluded as they may have affected by overprinting of various factors as we discussed above.

5.2. Positive Ce anomaly

A positive Ce anomaly represents enrichment in Ce above that expected based on the concentration of neighbouring REY. Ce is controlled by the adsorption/desorption processes into the surface of metal-oxide coatings of particles (Liu et al., 1988). The oxidized Ce^{4+} is less soluble and more readily adsorbed onto the surface of Fe-Mn oxides particles than Ce^{3+}. This would leave residual seawater depleted in Ce relative to other trivalent REEs, therefore the negative Ce anomaly indicates the oxygenation of the water mass (Alibo and Nozaki, 1999). The term “negative Ce anomaly” is widely acceptable as Ce/Ce*<0.9, but there is still uncertainty on accurately defining the positive Ce anomaly. Due to the fluctuations in Pr and Nd concentrations measured and the precision of ICP-MS analysis (accuracy within 5%), the Ce anomaly calculation may reach up to 1.2. To determine the true Ce enrichments, we make a statistics and find most data of Ce anomaly set within the threshold of 1.1 except four data exceed than 1.3. Therefore, the threshold is selected of 1.3 as the genuine positive Ce anomalies. When evaluating Ce anomaly data of the studied three sections, diagenetic and detrital effects have been excluded as discussed in section 4.1. The positive Ce anomalies show no correlation with Mn/Ca, Fe/Ca and Al/Ca, indicating minimal contamination from clay or Fe-Mn (oxyhydr) oxide phases (Fig. 4, 5). Positive Ce anomaly has been reported in some modern manganous waters (De Baar et al., 1988; De Carlo and Green, 2002) and also in some Proterozoic manganous deposits and carbonates (Mazumdar et al., 2003; Yu et al., 2016). As Wallace et al. (2017) indicated, positive Ce anomaly has been observed in the Sturtian and Marinoan glaciation termination. Hu et al. (2016), Ling et al., (2013) and Wang et al. (2014) reported positive Ce anomaly in cap carbonates of Jiulongwan section (Fig. 6). Meyer et al. (2012) also found the pink cap carbonates of post-Sturtian glaciation sharing the same positive Ce anomaly. All these data concur well with our results and convincingly support the genuine existence of positive Ce anomaly in cap carbonates.

The positive Ce anomaly and their causes thus provide us a unique opportunity to improve our understanding for the changes of the water mass redox conditions associated with the extreme post-Marinoan climatic changes. Factors that may influence the Ce mobility in the precipitation consist of the depositional ages (German and Elderfield, 1990), the pH values of water (Brookins, 1989; Stille et al., 1999; Tricca et al., 1999), the water depth (Wright et al., 1987; Piepgras and Jacobsen, 1992), the microbial mediation (Moffett, 1990), as well as the organic matters (Pourret et al., 2008) and Fe-Mn (oxyhydr) oixdes reductive dissolution

(Tostevin et al., 2016b). In the following, we will discuss these controlling factors in details:

(i) Changes induced by ages and precipitation depth

It has been identified that Ce seems to undergo progressive oxidative removal from the deep oceans during the ageing of individual water mass (German and Elderfield, 1990). Diffusion and bathymetry effects may contribute to REE heterogeneity within the same ocean basin. Ce anomaly would be affected by restricted stratified ocean and variation of depth and position. It is noted that transgression is occurred in the terminal Marinoan glaciation, whereas the studied three isochronous sections either present decreasing trend or steady curve (Fig. 2), in contradiction with the opinion that Ce/Ce^{*} ratios show a stepwise increasing trend with precipitation water depth during transgression (Ling et al., 2013).

(ii) Changes induced by alkalinity and organic matters

Positive Ce anomaly may be exhibited in organic-poor alkaline waters and alkaline lake waters due to preferential stabilization of carbonato-Ce(IV)-complexes by dissolved carbonates (Möller and Bau, 1993; Johannesson and Lyons, 1994; Davranche et al., 2005; Pourret et al., 2008). Deposition of cap carbonate is a response to a sudden increase in shallow-seawater alkalinity (Myrow and Kaufman, 1999; Shields, 2005). Independent evidence from boron isotope data of Xiaofenghe section in the Three Gorges area has been proposed that cap carbonate deposition experienced maximum ocean acidification event in the CA3 unit, and then returned to normalcy (Ohnemueller et al., 2014). Due to the total alkalinity (TA) would increase when pH rises, the pH and total alkalinity of the Doushantuo Member II should be higher than those of CA3 unit, and positive Ce anomaly should present, but such a shift is not supported by the Ce anomaly data in Doushantuo Member II samples. On the other hand, the bulk TOC data from Jiulongwan section show slightly decreasing trend during cap carbonates and fluctuate in Doushantuo Member II (McFadden et al., 2008), indicating lower organic matter content in the CA3 unit of cap carbonate in comparison with other units and Member II. As previous experiment ruled out, positive Ce anomaly may be developed in the organic-rich phases (Pourret et al., 2008), our data appear to object to the organic matter participating.

(iii) Changes induced by terrestrial input and diffusion effect

The observed positive Ce anomaly or no Ce anomaly in the shallow water of modern oxic ocean might be interpreted as resulting from terrestrial input (De Baar et al., 1985), due to the REY patterns from rivers or wind blown dust generally carry a flat REY signature, with LREE enriched and no fractionation between Ce and nearby REEs. However, Ce outlier of the Huajipo section presents an REY pattern with the depleted LREE relative to HREE (La/Yb<1) (Fig. 3c, f, i). If terrestrial inputs are anomalous mixed with seawater, the total REE content of carbonates would be higher (e.g., up to hundreds of ppm) and co-correlated higher Sc/Ca, which are absent in our studied samples. Moreover, if positive Ce anomaly results from excess continental input or inshore reducing sediments, the diffusion effect may affect Ce mobilization, and we would expect Ce enrichment to be most prevalent in alongshore section such as the Jiulongwan section. Although limited Ce enrichments are recorded in these sections, their values are more pronounced in offshore sections like Huajipo and Wuhe sections. Additionally, Le Hir et al. (2009) has deduced that the maximum dissolved elements from continental weathering into the ocean do not supply enough to be responsible for the elevated greenhouse in the period of cap carbonate deposition during the snowball melting. As fewer cations rushed into the ocean in the demise of cap carbonate deposition, then the positive Ce anomaly observed might not be the consequence of continental weathering input.

(iv) Changes induced by microbiological activity

Surface catalysis and biomineralization will affect the Ce behavior in the carbonatogenesis processes. The microbial oxidation that preferential scavenging of Ce(IV) could be a result of the negative Ce anomaly and little apparent Ce anomaly may occur in areas of high particle flux regions (Moffett, 1990). Recently, substantial fractionation of the REEs has been observed between the currently forming lacustrine stromatolites and the ambient waters, and the presence of putative microbialites exhibit HREE enrichments whereas the ambient waters are substantially HREE-depleted (Johannesson et al., 2014). However, based on the assumption that the REE of abiotic carbonate uptake from ambient waters without fractionation (Guido et al., 2011), if micro-biomineralization participated the cap carbonate deposition, the REE patterns of micrites and micritic dolomites should display HREE enriched pattern, but such REY patterns are not observed in our studied samples (La/Yb>1 and Gd/Yb>1 in JLW-18, HJP-18 and WH-16) (Fig. 3c, f, i). In addition, the presence of Fe-chelating siderophores, such as biogenic siderophore desferrioxamin-B (DFOB), can enhance the solubility of Ce(IV) and produce solutions with a positive Ce anomaly by partial dissolving volcanic ash particles and taking excess flux of dissolved REE into the ambient waters during the weathering of igneous rocks (Bau et al., 2013; Kraemer et al., 2015). The process may affect the input of REE into the ocean from continental weathering, but we find no anomalous Ce behavior in continental input (Fig.

4b, c). Further, the presence of biogenic chelators such as DFOB results in enriched Ce alongside La-depleted concave downward LREY pattern (Kraemer, 2004; Kraemer et al., 2015), which is in marked contrast to the positive La anomalies observed in the three sections (Fig. 3).

(v) Changes induced by release from Ce(IV) reduction

Positive Ce anomaly may be controlled by excess reductive Ce that releases from the oxide surface. The Ce(IV) forms separated solid oxide phase beneath the Ce redoxcline under oxic setting and independent of either Fe or Mn redox cycles (Haley et al., 2004). In this case, excess Ce(IV) would reduce to Ce(III), apart from the surface of oxide particles and release into ambient water, along with unfractionation of other REYs, including Y. However, Y/Ho ratios and positive Ce anomaly show a coupling increasing trend (Fig. 2), thus this speculation could be excluded.

(vi) Changes induced by dissolution of Fe-Mn-(oxyhydr) oxides

Excess Ce accumulation may also be attributed to reductive dissolution of Fe-Mn-(oxyhydr) oxides and release of all oxide bound REY. Detailed discussion will be demonstrated in below section.

5.3. Reductive dissolution of Mn- (oxyhydr) oxides

During the early diagenesis, REY released from reductive dissolution of Fe- or Mn-(oxyhydr) oxides in anoxic pore waters could be a potential mechanism for anomalous Ce behavior (Bau and Dulski, 1996; Haley et al., 2004). Fe-Mn (oxyhydr) oxides precipitated in seawater with initially colloidal particles as two major forms: hydrogenetic crusts and nodules.

The former usually are crustose shaped and develop above tholeiite and alkali basalt rocks, while the latter are concretions on the sea bed and accrete around a nucleus. The hydrogenetic crusts and nodules exist themselves in the seawater and are enriched in Co, a unique metal element that differs from hydrothermal and diagenetic fluids. So the observed higher Co/Ca ratios in CA3 units can be attributed to the accumulation process along with the dissolution of hydrogenetic Fe-Mn precipitates (Table 1). As proposed by Bau et al. (2014), the large data set point out that both hydrogenetic crusts and nodules show positive Ce anomaly, negative Y anomaly and high Nd concentration of >100 ppm. The positive Ce anomaly outliers drop on the seawater-hydrogenetic Fe-Mn nodules mixing curve (Fig. 7a, b), roughly 1%-8% hydrogenetic Fe-Mn nodules affect Nd concentration and 70% of those affect Y anomaly, suggesting a mixed-type hydrogenetic-seawater origin. Depleted HREE with positive Eu anomaly is indicative of hydrothermal influence, the entire samples are characterized by slight positive Eu anomalies (Fig. 3), this may indicate that the precipitation process is partly influenced by hydrothermal mixing. However, this process is incapable of the main positive Ce anomaly producer, because neither high-T hydrothermal fluid nor hydrothermal deposit could provide excess Ce and show positive Ce anomaly.

Mn-(oxyhydr) oxides may be considered as more important for controlling the redox cycling of Ce than Fe-(oxyhydr) oxides. Since the reduction potential of Ce(IV) (+1.6°V) is closer to Mn(IV) (+1.23°V) than Fe(III) (+0.77°V) (Randle and Kuhn, 1986; Lovley, 1991), Ce(III) adsorption and desorption tend to occur on Mn(II)/Mn(IV) transformation surface, rather than that of Fe(II)/Fe(III). The MREE-bulge patterns possibly result from preferential adsorption LREEs to Mn-(oxyhydr) oxides, as well as HREEs to Fe-(oxyhydr) oxides. The Fe-(oxyhydr) oxides often characterized by distinct MREE enrichment, high absolute Fe concentration and negative Y anomaly (Bau, 1999), while the dissolution of Mn-(oxyhydr) oxides may result in positive Ce anomaly alongside superchondritic Y anomaly, due to preferential adsorption of LREEs by Mn-(oxyhydr) oxides, and preferential scavenge MREEs by Fe-(oxyhydr) oxides, respectively (Gutjahr et al., 2007). Nevertheless, Fe-(oxyhydr) oxides may not be the primary carrier of Ce, as most evidence prove that the REY are scavenged onto Fe-(oxyhydr) oxides (Sholkovitz et al., 1994; De Carlo et al., 2000; Planavsky et al., 2010), without preferentially accumulating Ce. The Ce fractionation can only occur on the surface of Mn-(oxyhydr) oxides (Bau et al., 2014). Enriched MREEs and absolute high Fe concentration would occur in the water mass when encountered Fe(III)/Fe(II) dissolution. However, low Fe/Ca ratios, positive Y anomalies and normal $MREE/MREE^*$ are observed in JLW-18, HJP-18 and WH-16 (Fig. 3, Fig. 5e, Fig. 7c), in contrast to the reductive dissolution process of Fe-(oxyhydr) oxides. An alternative candidate may be the participating of Mn-(oxyhydr) oxides, whom can separately exist in a stable manganous zone on a dm-scale. Excess Ce may accumulate by reductive dissolution of Mn-(oxyhydr) oxides and release of all oxide bound REY in the form of $LnOH^{2+}$. The REY patterns of three outliers display positive Ce, La, Y, Eu anomalies alongside enriched HREE and no MREE anomalies (Fig. 3c, f, i), indicating a combination of seawater patterns via incorporating hydrogenetic Mn oxides REY across the Mn(IV/II) redoxcline, in agreement with the data from modern manganous zones with positive La, Y and Ce anomalies (De Carlo and Green, 2002). Additionally, elevated Mn/Fe ratios coupled with positive Ce anomalies (Fig. 7d) imply that Mn(II) together with redundant Ce exfoliate from the Mn-(oxyhydr) oxides that fallen from the shallow oxygenated surface water, further confirming the critical role of Mn-(oxyhydr) oxides in Ce cycling.

5.4. Redox model and palaeo environmental implications

The presence of Mn oxides is controlled by the oxidation state of the fluid, providing the link between oxygenation and Ce depletion. At the start of cap carbonate deposition, the flat or LREE-depleted REY patterns of CA1 and CA2 units present a seawater-glacial melting water mixing origin (Fig. 3). Normal Ce/Ce^* values are coupled with Fe speciation data ($Fe_{HR}/Fe_T > 0.38$, $Fe_{py}/Fe_{HR} < 0.7$) (Li et al., 2010) from Jiulongwan cap carbonates (Fig. 6). As defined by Tostevin et al. (2016), these data may indicate that the ocean initially was dominated anoxic ferruginous. Original Mn-(oxyhydr) oxides form in the shallow oxic waters with a positive Ce anomaly, leaving seawater with a negative anomaly, as the negative Ce anomalies ($Ce/Ce^*<0.9$) shown in Member II of Doushantuo carbonates. After the quickly initial surface complexation of Ce(III) on hydrogenetic Mn oxides, Ce is partially oxidized from Ce(III) to insoluble Ce(IV) with the catalyst of Mn(IV) at the metal (oxyhydr) oxide surface. The tetravalent Ce no longer participates once the exchange equilibrium between REY surface-complexes and REY solution-complexes reached. This equilibrium process is attained within several days (Ohta and Kawabe, 2001). Sequentially, a fraction of the scavenged Ce remains as Ce(IV) on the particles' surface. With time, Mn-(oxyhydr) oxides preferentially accumulate Ce over the other REY. Accompanying with the Mn-(oxyhydr) oxides across the Mn(IV)/Mn(II) redoxcline, excess Ce and dissolved Mn(II) release to the ambient water, which eventually results in the positive Ce anomaly observed in the CA3 unit of cap carbonates. Despite the absence of Fe speciation data from Huajipo and Wuhe cap carbonates, there is an equivocal discrimination area about the exact redox condition, we still deduce an existence of partial manganous zone from the positive Ce anomalies and relative REY signatures. Hence, the wedge that undergo Mn-(oxyhydr) oxides reductive dissolution sandwiches between well oxygenated and anoxic ferruginous water mass, indicating an intermediate manganous condition (Fig. 8), and in accordance with the positive Ce anomaly exhibited beneath Mn(IV)/Mn(II) redoxcline in modern manganous water (Bau et al., 1997; De Carlo and Green, 2002).

Eukaryote, especially large skeletal metazoan, mostly require oxygen to go aerobic respiration and collagen combination (Berkner and Marshall, 1965; Towe, 1970), for instance, modern skeletons and large animals sustain their survival function at the minimum DO constraint of 13 μM and 45 μM, respectively (Savrda and Bottjer, 1991; Levin et al., 2000). However, some metazoan, without complex motility and structure and owing coelom and circulatory system in small body size, can still survive under dysoxic or even anoxic environment. For instance, benthic sessile filter feeding demosponge, *Halichondria panacea*, could survive in the DO level of 2 μM to 16 μM (Mills et al., 2014). Nevertheless, typical case cannot blind the truths that massive mortality of meiofauna during the severe dysoxic condition (DO: 22.5~45 μM) (Diaz and Rosenberg, 1995), not to mention the mortality occurrence of Ediacaran soft-bodied biota or Cambrian large skeletal animals below DO with 90 μM (Canfield et al., 2007; Vaquer-Sunyer and Duarte, 2008; Zhang and Cui, 2016). In this case, well-oxygenated water provides essential habitat for these large metazoans (Penny et al., 2014). Mn reductive dissolution can steadily exist within the oceanic dissolved O_2 (DO) ranges from 10 μM to 100 μM (Klinkhammer and Bender, 1980; Johnson, 1992), so redox condition of extreme dysoxic to dysoxic is favored by the DO threshold to proceed Mn(IV)/Mn(II) reductive transformation (Tyson and Pearson, 1991). Ce is preferentially reduced than Mn due to the higher reduction potential of Ce and so excess Ce(III) can be released within the minimum DO threshold as 10 μM. Therefore, a transitive manganous wedge represents very limited O_2 concentration in comparison with the surface water (oxic, 210 μM DO at 25 ℃ and 35‰ salinity) and deep ferruginous water (anoxic, 0 μM DO). Assuming 10 μM as the maximum O_2 for Mn and Ce reduction, the manganous wedge thus explains the absence of high-oxygen needed biota and insufficient ability to meet habitable space for early animals.

Marinoan cap carbonate marks the first stage of rebuilding oxygen level and ecological environment in the aftermath of the Snowball Earth. If very limited evidence supports the appearance of possible biomarker like demosponge in the initial ocean (Love et al., 2009), then the found earliest fossil records large acanthomorphic acritarchs at the lower Member II of Doushantuo Formation (Yin et al., 2007), as is inferred as early cleavage embryos of large animals (Cohen et al., 2009; Willman, 2009). Of note, independently Zn isotope data show an elevated trend from the middle unit of cap carbonates and reveal the recovery of primary production and nutrients supply in this time interval (Kunzmann et al., 2013). Additionally, evidence from Se and Mo isotopes decode the increased ocean oxidation in the upper Doushantuo Formation, in consistent with the stepwise oxygenation for rehabilitation of skeletal animals and complex ecologies (Chen et al., 2015; Pogge von Strandmann et al., 2015). Consequently, the transitive manganous wedge in the demise of cap carbonate deposition, acts as O_2 recovery channel, implying the redox condition from anoxic ferruginous transforming to dysoxic phase and thus restricting the habitat space for early Ediacaran biota.

6. Conclusions

Our integrated shelf-basin wide chemostratigraphic correlations of the Ediacaran cap carbonates based on time-series Ce anomaly and REY proxies present compelling positive Ce anomalies ($Ce/Ce^{*}>1.3$) in the demise of cap carbonate deposition. This finding suggests that a surplus of Ce released to ambient water along with the reductive dissolution of Mn-(oxyhydr) oxides in the low-oxygen manganous wedge (DO ~10 μM), whom sandwiched between well oxygenated water and anoxic ferruginous deep water. In the demise of Marinoan cap carbonate deposition, the intermediate manganous zone acts as O_2 recovery channel, implying the redox condition from anoxic ferruginous transforming to dysoxic phase and thus restricting the habitat space for early Ediacaran biota. Future work is recommended to optimize the high-precision Fe species and redox- sensitive Mo isotope measurement of cap carbonates, so as to further synthesizing the certain redox condition. In spite of the limitation mentioned above, our study provides a novel springboard to better understanding the relationship between oceanic dissolved O_2 constraint and early metazoan appearance.

Acknowledgements

This research is made benefited from the constructive suggestions from Dr. Rosalie Tostevin and He Tian-Chen. The authors are grateful to Professor Zhu Maoyan and Dr. Lv Miao (Nanjing Institute of Geology and Palaeontology, China) for their help in the sample supports and stratigraphical discussion. Dr Matthew Cooper and Ms Agnieszka Michalik (National Oceanography Centre, UK) are acknowledged with support for elements analysis. This research is funded by the National Science Foundation of China (No.41230102) and the scholarship from China Scholarship Council.

References

Alibo, D.S., Nozaki, Y., 1999. Rare earth elements in seawater: particle association, shale-normalization, and Ce oxidation. Geochim. Cosmochim. Acta. 63, 363-372.

Arslan, Z., Paulson, A.J., 2003. Solid phase extraction for analysis of biogenic carbonates by electrothermal vaporization inductively coupled plasma mass spectrometry (ETV-ICP-MS): an investigation of rare earth element signatures in otolith microchemistry. Anal. Chim. Acta.476, 1-13.

Banner J.L, Hanson.G.N., Meyers W.J., 1988. Rare earth element and Nd isotopic variations in regionally extensive dolomites from the Burlington-Keokuk Formation (Mississippian): Implications for REE mobility during carbonate diagenesis. J. Sediment. Res. 58, 415-432.

Bau, M., 1991. Rare-earth element mobility during hydrothermal and metamorphic fluid-rock interaction and the significance of the oxidation state of europium. Chem. Geol. 93, 219-230.

Bau, M., 1999. Scavenging of dissolved yttrium and rare earths by precipitating iron oxyhydroxide: experimental evidence for Ce oxidation, Y-Ho fractionation, and lanthanide tetrad effect. Geochim. Cosmochim. Acta. 63, 67-77.

Bau, M., Dulski, P., 1996. Distribution of yttrium and rare-earth elements in the Penge and Kuruman iron-formations, Transvaal Supergroup, South Africa. Precambrian.Res 79, 37-55.

Bau, M., Möller, P., Dulski, P., 1997. Yttrium and lanthanides in eastern Mediterranean seawater and their fractionation during redox-cycling. Mar. Chem. 56, 123-131.

Bau, M., Schmidt, K., Koschinsky, A., Hein, J., Kuhn, T., Usui, A., 2014. Discriminating between different genetic types of marine ferro-manganese crusts and nodules based on rare earth elements and yttrium. Chem. Geol. 381, 1-9.

Bau, M., Tepe, N., Mohwinkel, D., 2013. Siderophore-promoted transfer of rare earth elements and iron from volcanic ash into glacial meltwater, river and ocean water. Earth. Planet. Sci. Lett. 364, 30-36.

Bechstädt, T., Jägera, H., Rittersbacherb, A., Schweisfurthc B., Spenced, G., Wernere, G., Bonif, M., 2018. The Cryogenian Ghaub Formation of Namibia － New insights into Neoproterozoic glaciations. Earth-Science Reviews 177, 678-714.

Berkner, L.V., Marshall, L.C., 1965. On the Origin and Rise of Oxygen Concentration in the Earth's Atmosphere. J. Atmos Sci. 22, 225-261.

Bodin, S., Godet, A., Matera, V., Steinmann, P., Vermeulen, J., Gardin, S., Adatte, T., Coccioni, R., Föllmi, K.B., 2007. Enrichment of redox-sensitive trace metals (U, V, Mo, As) associated with the late Hauterivian Faraoni oceanic anoxic event. Int. J. Earth Sci. 96, 327-341.

Böning, P., Brumsack, H.-J., Böttcher, M.E., Schnetger, B., Kriete, C., Kallmeyer, J., Borchers, S.L., 2004. Geochemistry of Peruvian near-surface sediments. Geochim. Cosmochim. Acta. 68, 4429-4451

Brookins, D., 1989. Aqueous geochemistry of rare earth elements. Rev. Mineral. Geochem.21, 201-225.

Calvert, S.E., Pedersen, T.F., 1993. Geochemistry of recent oxic and anoxic marine sediments: implications for the geological record. Mar. Geol. 113, 67-88.

Campbell, A., Palmer, M., Klinkhammer, G., Bowers, T., Edmond, J., Lawrence, J., Casey, J., Thompson, G., Humphris, S., Rona, P., 1988. Chemistry of hot springs on the Mid-Atlantic Ridge. Nature 335, 514-519.

Canfield, D.E., Poulton, S.W., Narbonne, G.M., 2007. Late-Neoproterozoic Deep-Ocean Oxygenation and the Rise of Animal Life. Science 315, 92-95.

Caxito, F.A., Halverson, G.P., Uhlein, A., Stevenson, R., Dias, T.G., Uhlein, G.J., 2012. Marinoan glaciation in east central Brazil. Precambrian Res. 200-203, 38-58.

Caxito, F.A., Frei, R., Uhlein, G.J., Dias, T.G., Árting, T.B., Uhlein, A., 2018. Multiproxy geochemical and isotope stratigraphy records of a Neoproterozoic Oxygenation Event in the Ediacaran Sete Lagoas cap carbonate, Bambuí Group, Brazil. Chem. Geol.

https://doi.org/10.1016/j.chemgeo.2018.02.007.

Chen, J., Algeo, T.J., Zhao, L., Chen, Z.-Q., Cao, L., Zhang, L., Li, Y., 2015. Diagenetic uptake of rare earth elements by bioapatite, with an example from Lower Triassic conodonts of South China. Earth-Sci. Rev. 149, 181-202.

Chen, X., Ling, H.-F., Vance, D., Shields-Zhou, G.A., Zhu, M., Poulton, S.W., Och, L.M., Jiang, S.-Y., Li, D., Cremonese, L., Archer, C., 2015. Rise to modern levels of ocean oxygenation coincided with the Cambrian radiation of animals. Nat. Commun. 6, 7142-7149.

Cohen, P.A., Knoll, A.H., Kodner, R.B., 2009. Large spinose microfossils in Ediacaran rocks as resting stages of early animals. P. Natl. Acad. Sci. USA. 106, 6519-6524.

Condon, D., Zhu, M., Bowring, S., Wang, W., Yang, A., Jin, Y., 2005. U-Pb ages from the neoproterozoic Doushantuo Formation, China. Science 308, 95-98.

Davranche, M., Pourret, O., Gruau, G., Dia, A., Le Coz-Bouhnik, M., 2005. Adsorption of REE(III)-humate complexes onto MnO_2: Experimental evidence for cerium anomaly and lanthanide tetrad effect suppression. Geochim. Cosmochim. Acta. 69, 4825-4835.

De Baar, H.J., German, C.R., Elderfield, H., Van Gaans, P., 1988. Rare earth element distributions in anoxic waters of the Cariaco Trench. Geochimica et Cosmochimica Acta. 52, 1203-1219.

De Baar, H.J.W., Bacon, M.P., Brewer, P.G., Bruland, K.W., 1985. Rare earth elements in the Pacific and Atlantic Oceans. Geochim. Cosmochim. Acta. 49, 1943-1959.

De Carlo E.R, Wen.X.Y., Cowen, J.P., 2000. Rare earth element fractionation in hydrogenetic Fe-Mn crusts: The influence of carbonate complexation and phosphatization on Sm/Yb ratios.Soc. Sediment. Geol. 66, 271-285.

De Carlo, E.H., Green, W.J., 2002. Rare earth elements in the water column of Lake Vanda, McMurdo Dry Valleys, Antarctica. Geochim. Cosmochim. Acta. 66, 1323-1333.

Derry, L.A., Brasier, M.D., Corfield, R.M., Rozanov, A.Y., Zhuravlev, A.Y., 1994. Sr and C isotopes in Lower Cambrian carbonates from the Siberian craton: a paleoenvironmental record during the ‘Cambrian explosion’. Earth. Planet. Sci. Lett. 128, 671-681.

Diaz, R.J., Rosenberg,R., 1995. Marine benthic hypoxia: A review of its ecological e ects and the behavioural responses of benthic macrofauna. Oceanogr. Mar. Biol. Annu. Rev. 33, 245-303.

Font, E., Nédélec, A., Trindade, R., Macouin, M., Charrière, A., 2006. Chemostratigraphy of the Neoproterozoic Mirassol d'Oeste cap dolostones (Mato Grosso, Brazil): An alternative model for Marinoan cap dolostone formation. Earth. Planet. Sci. Lett. 250, 89-103.

Font, E., Nédélec, A., Trindade, R.I.F., Moreau, C., 2010. Fast or slow melting of the Marinoan snowball Earth? The cap dolostone record. Palaeogeogr. Palaeoclimatol. Palaeoecol. 295, 215-225.

German, C.R., Elderfield, H., 1990. Application of the Ce anomaly as a paleoredox indicator: the ground rules. Paleoceanography 5, 823-833.

Guido, A., Mastandrea, A., Tosti, F., Russo, F., 2011. Importance of rare earth element patterns in discrimination between biotic and abiotic mineralization, Advances in Stromatolite Geobiology. Springer, pp. 453-462.

Gutjahr, M., Frank, M., Stirling, C.H., Klemm, V., van de Flierdt, T., Halliday, A.N., 2007.

Reliable extraction of a deepwater trace metal isotope signal from Fe–Mn oxyhydroxide coatings of marine sediments. Chem. Geol. 242, 351-370.

Haley, B.A., Klinkhammer, G.P., McManus, J., 2004. Rare earth elements in pore waters of marine sediments. Geochim. Cosmochim. Acta. 68, 1265-1279.

Higgins, J.A., Schrag, D.P., 2003. Aftermath of a snowball Earth. Geochem. Geophys. Geosyst. 4, 1-20.

Hoffman, P.F., Kaufman, A.J., Halverson, G.P., Schrag, D.P., 1998. A Neoproterozoic snowball earth. Science 281, 1342-1346.

Hoffmann, K.-H., Condon, D., Bowring, S., Crowley, J., 2004. U-Pb zircon date from the Neoproterozoic Ghaub Formation, Namibia: constraints on Marinoan glaciation. Geology 32, 817-820.

Hu, R., Wang, W., Li, S.-Q., Yang, Y.-Z., Chen, F., 2016. Sedimentary Environment of Ediacaran Sequences of South China: Trace Element and Sr-Nd Isotope Constraints. J. Geol. 124, 769-789.

Huang, J., Chu, X., Chang, H., Feng, L., 2009. Trace element and rare earth element of cap carbonate in Ediacaran Doushantuo Formation in Yangtze Gorges. Chin. Sci. Bull. 54, 3295-3302.

Huang, J., Chu, X., Jiang, G., Feng, L., Chang, H., 2011. Hydrothermal origin of elevated iron, manganese and redox-sensitive trace elements in the c. 635 Ma Doushantuo cap carbonate. J. Geol. Soc. London. 168, 805-816.

Hurtgen, M.T., Halverson, G.P., Arthur, M.A., Hoffman, P.F., 2006. Sulfur cycling in the aftermath of a 635-Ma snowball glaciation: Evidence for a syn-glacial sulfidic deep ocean. Earth. Planet. Sci. Lett. 245, 551-570.

Hyde, W.T., Crowley, T.J., Baum, S.K., Peltier, W.R., 2000. Neoproterozoic ‘snowball Earth’simulations with a coupled climate/ice-sheet model. Nature 405, 425-429.

Jacobsen, S.B., Kaufman, A.J., 1999. The Sr, C and O isotopic evolution of Neoproterozoic seawater. Chem. Geol. 161, 37-57.

James, N.P., Narbonne, G.M., Kyser, T.K., 2001. Late Neoproterozoic cap carbonates: Mackenzie Mountains, northwestern Canada: precipitation and global glacial meltdown. Can. J. Earth Sci. 38, 1229-1262.

James, R., Elderfield, H., Palmer, M., 1995. The chemistry of hydrothermal fluids from the Broken Spur site, 29 N Mid-Atlantic Ridge. Geochim. Cosmochim. Acta. 59, 651-659.

Jiang, G., Kaufman, A.J., Christie-Blick, N., Zhang, S., Wu, H., 2007. Carbon isotope variability across the Ediacaran Yangtze platform in South China: Implications for a large surface-to-deep ocean $\delta^{13}C$ gradient. Earth. Planet. Sci. Lett. 261, 303-320.

Jiang, G., Kennedy, M.J., Christie-Blick, N., 2003. Stable isotopic evidence for methane seeps in Neoproterozoic postglacial cap carbonates. Nature 426, 822-826.

Jiang, G., Kennedy, M.J., Christie-Blick, N., Wu, H., Zhang, S., 2006. Stratigraphy, sedimentary structures, and textures of the late Neoproterozoic Doushantuo cap carbonate in South China. J.Sedimentary Res. 76, 978-995.

Jiang, S.-Y., Zhao, H.-X., Chen, Y.-Q., Yang, T., Yang, J.-H., Ling, H.-F., 2007. Trace and rare earth element geochemistry of phosphate nodules from the lower Cambrian black shale sequence in the Mufu Mountain of Nanjing, Jiangsu province, China. Chem. Geol. 244, 584-604.

Johannesson, K.H., Hawkins, D.L., Cortés, A., 2006. Do Archean chemical sediments record ancient seawater rare earth element patterns? Geochim. Cosmochim. Acta. 70, 871-890.

Johannesson, K.H., Lyons, W.B., 1994. The rare earth element geochemistry of Mono Lake water and the importance of carbonate complexing. Limnol. Oceanogr. 39, 1141-1154.

Johannesson, K.H., Telfeyan, K., Chevis, D.A., Rosenheim, B.E., Leybourne, M.I., 2014. Rare earth elements in stromatolites—1. Evidence that modern terrestrial stromatolites fractionate rare earth elements during incorporation from ambient waters, Evolution of Archean Crust and Early Life. Springer, pp. 385-411.

Johnson, K.S., 1992. Manganese flux from continental margin sediments in a transect through the oxygen minimum. Science 257, 1242-1245.

Kennedy, M.J., Runnegar, B., Prave, A.R., Hoffmann, K.H., Arthur, M.A., 1998. Two or four Neoproterozoic glaciations? Geology 26, 1059-1063.

Kirschvink, J.L., 1992. Late Proterozoic low-latitude global glaciation: the snowball Earth. Geological Evolution of the Proterozoic Earth. Cambridge University Press, pp. 51-52.

Klinkhammer, G.P., Bender, M.L., 1980. The distribution of manganese in the Pacific Ocean. Earth. Planet. Sci. Lett. 46, 361-384.

Kraemer, D., Kopf, S., Bau, M., 2015. Oxidative mobilization of cerium and uranium and enhanced release of “immobile” high field strength elements from igneous rocks in the presence of the biogenic siderophore desferrioxamine B. Geochim. Cosmochim. Acta. 165, 263-279.

Kraemer, S.M., 2004. Iron oxide dissolution and solubility in the presence of siderophores. Aquat. Sci. 66, 3-18.

Kunzmann, M., Halverson, G.P., Sossi, P.A., Raub, T.D., Payne, J.L., Kirby, J., 2013. Zn isotope evidence for immediate resumption of primary productivity after snowball Earth. Geology 41, 27-30.

Lawrence, M.G., Greig, A., Collerson, K.D., Kamber, B.S., 2006. Rare earth element and yttrium variability in South East Queensland waterways. Aquat. Geochem. 12, 39-72.

Le Hir, G., Donnadieu, Y., Goddéris, Y., Pierrehumbert, R.T., Halverson, G.P., Macouin, M., Nédélec, A., Ramstein, G., 2009. The snowball Earth aftermath: Exploring the limits of continental weathering processes. Earth. Planet. Sci. Lett. 277, 453-463.

Lécuyer, C., Bogey, C., Garcia, J.-P., Grandjean, P., Barrat, J.-A., Floquet, M., Bardet, N., Pereda-Superbiola, X., 2003. Stable isotope composition and rare earth element content of vertebrate remains from the Late Cretaceous of northern Spain (Laño): did the environmental record survive? Palaeogeogr. Palaeoclimatol. Palaeoecol. 193, 457-471.

Levin, L.A., Gage, J.D., Martin, C., Lamont, P.A., 2000. Macrobenthic community structure within and beneath the oxygen minimum zone, NW Arabian Sea. Deep-Sea. Res. Pt II. 47, 189-226.

Li, C., Love, G.D., Lyons, T.W., Fike, D.A., Sessions, A.L., Chu, X., 2010. A stratified redox model for the Ediacaran ocean. Science 328, 80-83.

Ling, H.-F., Chen, X., Li, D., Wang, D., Shields-Zhou, G.A., Zhu, M., 2013. Cerium anomaly variations in Ediacaran–earliest Cambrian carbonates from the Yangtze Gorges area, South China: Implications for oxygenation of coeval shallow seawater. Precambrian. Res. 225, 110-127.

Liu, X., Byrne, R.H., 1995. Comparative carbonate complexation of yttrium and gadolinium at 25 ℃and 0.7 mol dm^{-3} ionic strength. Mar. Chem. 51, 213-221.

Liu, Y.-G., Miah, M., Schmitt, R., 1988. Cerium: a chemical tracer for paleo-oceanic redox conditions. Geochim. Cosmochim. Acta. 52, 1361-1371.

Lorentz, N.J., Corsetti, F.A., Link, P.K., 2004. Seafloor precipitates and C-isotope stratigraphy from the Neoproterozoic Scout Mountain Member of the Pocatello Formation, southeast Idaho: implications for Neoproterozoic earth system behavior. Precambrian. Res. 130, 57-70.

Love, G.D., Grosjean, E., Stalvies, C., Fike, D.A., Grotzinger, J.P., Bradley, A.S., Kelly, A.E., Bhatia, M., Meredith, W., Snape, C.E., Bowring, S.A., Condon, D.J., Summons, R.E., 2009. Fossil steroids record the appearance of Demospongiae during the Cryogenian period. Nature 457, 718-721.

Lovley, D.R., 1991. Dissimilatory Fe (III) and Mn (IV) reduction. Microbiol. Rev. 55, 259-287.

Lu, M., Zhu, M.Y., Zhang, J.M., Shields-Zhou, G., Li, G.X., Zhao, F.C., Zhao, X., Zhao, M.J., 2013. The DOUNCE event at the top of the Ediacaran Doushantuo Formation, South China: Broad stratigraphic occurrence and non-diagenetic origin. Precambrian. Res. 225, 86-109.

Mazumdar, A., Tanaka, K., Takahashi, T., Kawabe, I., 2003. Characteristics of rare earth element abundances in shallow marine continental platform carbonates of Late

Neoproterozoic successions from India. Geochem. J. 37, 277-289.

McFadden, K.A., Huang, J., Chu, X., Jiang, G., Kaufman, A.J., Zhou, C., Yuan, X., Xiao, S., 2008. Pulsed oxidation and biological evolution in the Ediacaran Doushantuo Formation. P. Natl. Acad. Sci. USA. 105, 3197-3202.

McLennan, S., 1989. Rare earth elements in sedimentary rocks; influence of provenance and sedimentary processes.Rev. Mineral. Geochem. 21, 169-200.

Meyer, E.E., Quicksall, A.N., Landis, J.D., Link, P.K., Bostick, B.C., 2012. Trace and rare earth elemental investigation of a Sturtian cap carbonate, Pocatello, Idaho: evidence for ocean redox conditions before and during carbonate deposition. Precambrian. Res. 192, 89-106.

Michard, A., Albarede, F., 1986. The REE content of some hydrothermal fluids. Chem. Geol. 55, 51-60.

Mills, D.B., Ward, L.M., Jones, C., Sweeten, B., Forth, M., Treusch, A.H., Canfield, D.E., 2014. Oxygen requirements of the earliest animals. P. Natl. Acad. Sci. USA. 111, 4168-4172.

Moffett, J.W., 1990. Microbially mediated cerium oxidation in sea water. Nature 345, 421-423.

Möller, P., Bau, M., 1993. Rare-earth patterns with positive cerium anomaly in alkaline waters from Lake Van, Turkey. Earth. Planet. Sci. Lett. 117, 671-676.

Morford, J., Russell, A., Emerson, S., 2001. Trace metal evidence for changes in the redox environment associated with the transition from terrigenous clay to diatomaceous sediment, Saanich Inlet, BC. Mar. Geol. 174, 355-369.

Murray, R.W., Buchholtz Ten Brink, M.R., Gerlach, D.C., Russ III, G.P., Jones, D.L., 1991. Rare earth, major, and trace elements in chert from the Franciscan Complex and Monterey

Group, California: Assessing REE sources to fine-grained marine sediments. Geochim. Cosmochim. Acta. 55, 1875-1895.

Myrow, P.M, Kaufman, A.J., 1999. A newly discovered cap carbonate above Varanger-age glacial deposits in Newfoundland, Canada. J. Sediment Res. 69, 784-793.

Nothdurft, L.D., Webb, G.E., Kamber, B.S., 2004. Rare earth element geochemistry of Late Devonian reefal carbonates, Canning Basin, Western Australia: confirmation of a seawater REE proxy in ancient limestones. Geochim. Cosmochim. Acta. 68, 263-283.

Nozaki, Y., Zhang, J., 1995. The rare earth elements and yttrium in the coastal/offshore mixing zone of Tokyo Bay waters and the Kuroshio. Biogeochemical Processes and Ocean Flux in the Western Pacific. Terra Scientific Publishing, pp. 171-184.

Nozaki, Y., Zhang, J., Amakawa, H., 1997. The fractionation between Y and Ho in the marine environment. Earth. Planet. Sci. Lett. 148, 329-340.

Ohnemueller, F., Prave, A.R., Fallick, A.E., Kasemann, S.A., 2014. Ocean acidification in the aftermath of the Marinoan glaciation. Geology 42, 1103-1106.

Ohta, A., Kawabe, I., 2001. REE(III) adsorption onto Mn dioxide (δ-MnO_2) and Fe oxyhydroxide: Ce(III) oxidation by δ-MnO_2. Geochim. Cosmochim. Acta. 65, 695-703.

Parekh, P.P., Möller, P., Dulski, P., Bausch, W.M., 1977. Distribution of trace elements between carbonate and non-carbonate phases of limestone. Earth. Planet. Sci. Lett. 34, 39-50.

Penny, A.M., Wood, R., Curtis, A., Bowyer, F., Tostevin, R., Hoffman, K.H., 2014. Ediacaran metazoan reefs from the Nama Group, Namibia. Science 344, 1504-1506.

Piepgras, D.J., Jacobsen, S.B., 1992. The behavior of rare earth elements in seawater: Precise determination of variations in the North Pacific water column. Geochim. Cosmochim. Acta. 56, 1851-1862.

Planavsky, N., Bekker, A., Rouxel, O.J., Kamber, B., Hofmann, A., Knudsen, A., Lyons, T.W., 2010. Rare Earth Element and yttrium compositions of Archean and Paleoproterozoic Fe formations revisited: New perspectives on the significance and mechanisms of deposition. Geochim. Cosmochim. Acta. 74, 6387-6405.

Pogge von Strandmann, P.A.E., Stüeken, E.E., Elliott, T., Poulton, S.W., Dehler, C.M., Canfield, D.E., Catling, D.C., 2015. Selenium isotope evidence for progressive oxidation of the Neoproterozoic biosphere. Nat. Commun. 6, 10157-10167.

Pourmand, A., Dauphas, N., Ireland, T.J., 2012. A novel extraction chromatography and MC-ICP-MS technique for rapid analysis of REE, Sc and Y: Revising CI-chondrite and Post-Archean Australian Shale (PAAS) abundances. Chem. Geol. 291, 38-54.

Pourret, O., Davranche, M., Gruau, G., Dia, A., 2008. New insights into cerium anomalies in organic-rich alkaline waters. Chem. Geol. 251, 120-127.

Pujol, F., Berner, Z., Stüben, D., 2006. Palaeoenvironmental changes at the Frasnian/Famennian boundary in key European sections: chemostratigraphic constraints. Palaeogeogr. Palaeoclimatol. Palaeoecol. 240, 120-145.

Randle, T.H., Kuhn, A.T., 1986. The influence of platinum (phase) oxide on the electrode kinetics of the manganese(III)/manganese(II) and cerium(IV)/cerium(III) redox couples in sulphuric acid. Electrochim. Acta 31, 739-744.

Reynard, B., Lécuyer, C., Grandjean, P., 1999. Crystal-chemical controls on rare-earth element concentrations in fossil biogenic apatites and implications for paleoenvironmental reconstructions. Chem. Geol. 155, 233-241.

Rose, C.V., Maloof, A.C., 2010. Testing models for post-glacial ‘cap dolostone’ deposition: Nuccaleena Formation, South Australia. Earth. Planet. Sci. Lett. 296, 165-180.

Sarangia, S., Mohanty, S.P., Barik, A., 2017. Rare earth element characteristics of Paleoproterozoic cap carbonates pertaining to the Sausar Group, Central India: Implications for ocean paleoredox conditions. J. Asian Earth Sci. 148, 31-50.

Savrda, C.E., Bottjer, D.J., 1991. Oxygen-related biofacies in marine strata: an overview and update. Geol. Soc. London. Spec. Publ. 58, 201-219.

Schröder, S., Grotzinger, J., 2007. Evidence for anoxia at the Ediacaran-Cambrian boundary: the record of redox-sensitive trace elements and rare earth elements in Oman. J. Geol. Soc. London. 164, 175-187.

Shields, G., Stille,P., Brasier, M. D., Atudorei, N., 1997. Stratified oceans and oxygenation of the late Precambrian environment: a post glacial geochemical record from the Neoproterozoic of W. Mongolia. Terra Nova 9, 218-222.

Shields, G., Stille, P., 2001. Diagenetic constraints on the use of cerium anomalies as palaeoseawater redox proxies: an isotopic and REE study of Cambrian phosphorites. Chem. Geol. 175, 29-48.

Shields, G.A., 2005. Neoproterozoic cap carbonates: a critical appraisal of existing models and the plumeworld hypothesis. Terra Nova 17, 299-310.

Shields, G.A., Webb, G.E., 2004. Has the REE composition of seawater changed over geological time? Chem. Geol. 204, 103-107.

Sholkovitz, E.R., Landing, W.M., Lewis, B.L., 1994. Ocean particle chemistry: The fractionation of rare earth elements between suspended particles and seawater. Geochim. Cosmochim. Acta. 58, 1567-1579.

Song, H., Wignall, P.B., Tong, J., Bond, D.P.G., Song, H., Lai, X., Zhang, K., Wang, H., Chen, Y., 2012. Geochemical evidence from bio-apatite for multiple oceanic anoxic events during Permian-Triassic transition and the link with end-Permian extinction and recovery. Earth. Planet. Sci. Lett. 353, 12-21.

Stille, P., Gauthier-Lafaye, F., Louvat, D., 1999. REE migration in groundwaters close to the natural fission reactor of Bangombé (Gabon); Sm-Nd isotope evidence, Proc. of the Oklo Phase II Workshop (eds. D. Louvat, V. Michaud and Hv Maravic). EUR Report Series, pp. 263-272.

Taylor, S.R., McLennan, S.M., 1985. The continental crust: its composition and evolution. Blackwell, pp. 57-72.

Tessier, A., Campbell, P.G., Bisson, M., 1979. Sequential extraction procedure for the speciation of particulate trace metals. Anal. Chem. 51, 844-851.

Tian, X., Luo, K., Wang, S., Ni, R., 2014. Geochemical characteristics of trace elements and rare earth elements during the Cryogenian-Ediacaran transition in Yangtze Gorges area. J. Palaeogeogr. 16, 483-502 (in Chinese with English Abstract).

Tostevin, R., Shields, G.A., Tarbuck, G.M., He, T., Clarkson, M.O., Wood, R.A., 2016a. Effective use of cerium anomalies as a redox proxy in carbonate-dominated marine settings.

Chem. Geol. 438, 146-162.

Tostevin, R., Wood, R.A., Shields, G.A., Poulton, S.W., Guilbaud, R., Bowyer, F., Penny, A.M., He, T., Curtis, A., Hoffmann, K.H., Clarkson, M.O., 2016b. Low-oxygen waters limited habitable space for early animals. Nat. Commun. 7, 12818-12827.

Towe, K.M., 1970. Oxygen-Collagen Priority and the Early Metazoan Fossil Record. P. Natl. Acad. Sci. USA.65, 781-788.

Tribovillard, N., Algeo, T.J., Lyons, T., Riboulleau, A., 2006. Trace metals as paleoredox and paleoproductivity proxies: an update. Chem. Geol. 232, 12-32.

Tricca, A., Stille, P., Steinmann, M., Kiefel, B., Samuel, J., Eikenberg, J., 1999. Rare earth elements and Sr and Nd isotopic compositions of dissolved and suspended loads from small river systems in the Vosges mountains (France), the river Rhine and groundwater. Chem. Geol. 160, 139-158.

Tyson, R.V., Pearson, T.H., 1991. Modern and ancient continental shelf anoxia: an overview. Geol. Soc. London. Spec. Publ. 58, 1-24.

Vaquer-Sunyer, R., Duarte, C.M., 2008. Thresholds of hypoxia for marine biodiversity. P. Natl. Acad. Sci. USA.105, 15452-15457.

Vernhet, E., Heubeck, C., Zhu, M.Y., Zhang, J.M., 2006. Large-scale slope instability at the southern margin of the Ediacaran Yangtze platform (Hunan province, central China). Precambrian. Res. 148, 32-44.

Wallace, M.W., Hood, A.v., Shuster, A., Greig, A., Planavsky, N.J., Reed, C.P., 2017. Oxygenation history of the Neoproterozoic to early Phanerozoic and the rise of land plants.

Earth. Planet. Sci. Lett. 466, 12-19.

Wang, J., Jiang, G., Xiao, S., Li, Q., Wei, Q., 2008. Carbon isotope evidence for widespread methane seeps in the ca. 635 Ma Doushantuo cap carbonate in south China. Geology 36, 347-350.

Wang, J., Li, Z.-X., 2003. History of Neoproterozoic rift basins in South China: implications for Rodinia break-up. Precambrian. Res. 122, 141-158.

Wang, Q., Lin, Z., Chen, D., 2014. Geochemical constraints on the origin of Doushantuo cap carbonates in the Yangtze Gorges area, South China. Sediment. Geol. 304, 59-70.

Webb, G.E., Kamber, B.S., 2000. Rare earth elements in Holocene reefal microbialites: a new shallow seawater proxy. Geochim. Cosmochim. Acta. 64, 1557-1565.

Webb, G.E., Nothdurft, L.D., Kamber, B.S., Kloprogge, J., Zhao, J.X., 2009. Rare earth element geochemistry of scleractinian coral skeleton during meteoric diagenesis: a sequence through neomorphism of aragonite to calcite. Sedimentology 56, 1433-1463.

Willman, S., 2009. Morphology and wall ultrastructure of leiosphaeric and acanthomorphic acritarchs from the Ediacaran of Australia. Geobiology 7, 8-20.

Wright, J., Schrader, H., Holser, W.T., 1987. Paleoredox variations in ancient oceans recorded by rare earth elements in fossil apatite. Geochim. Cosmochim. Acta. 51, 631-644.

Wyndham, T., McCulloch, M., Fallon, S., Alibert, C., 2004. High-resolution coral records of rare earth elements in coastal seawater: biogeochemical cycling and a new environmental proxy. Geochim. Cosmochim. Acta. 68, 2067-2080.

Xin, H., Jiang, S.-Y., Yang, J.-H., Wu, H.-P., Pi, D.-H., 2015. Rare earth element and Sr–Nd isotope geochemistry of phosphatic rocks in Neoproterozoic Ediacaran Doushantuo Formation in Zhangcunping section from western Hubei Province, South China. Palaeogeogr. Palaeoclimatol. Palaeoecol. 440, 712-724.

Yan, B., Zhu, X., Tang, S., 2010. Characteristics of Sr Isotopes and Rare Earth Elements of Cap Carbonates in Doushantuo Formation in the Three Gorges Area. GeoSci. 24, 832-839 (in Chinese with English Abstract).

Yin, C., Tang, F., Liu, Y., Gao, L.-z., Liu, P.-j., Xing, Y., Yang, Z., Wan, Y., Wang, Z., 2005. U-Pb zircon age from the base of the Ediacaran Doushantuo Formation in the Yangtze Gorges, South China: constraint on the age of Marinoan glaciation. Episodes 28, 48-49.

Yin, L., Zhu, M., Knoll, A.H., Yuan, X., Zhang, J., Hu, J., 2007. Doushantuo embryos preserved inside diapause egg cysts. Nature 446, 661-663.

Yoshioka, H., Asahara, Y., Tojo, B., Kawakami, S.-i., 2003. Systematic variations in C, O, and Sr isotopes and elemental concentrations in Neoproterozoic carbonates in Namibia: implications for a glacial to interglacial transition. Precambrian. Res. 124, 69-85.

Yu, W., Algeo, T.J., Du, Y., Maynard, B., Guo, H., Zhou, Q., Peng, T., Wang, P., Yuan, L., 2016. Genesis of Cryogenian Datangpo manganese deposit: Hydrothermal influence and episodic post-glacial ventilation of Nanhua Basin, South China. Palaeogeogr. Palaeoclimatol. Palaeoecol. 459, 321-337.

Yuan, X., Chen, Z., Xiao, S., Zhou, C., Hua, H., 2011. An early Ediacaran assemblage of macroscopic and morphologically differentiated eukaryotes. Nature 470, 390-393.

Zhang, K., Zhu, X.-K., Yan, B., 2015. A refined dissolution method for rare earth element studies of bulk carbonate rocks. Chem. Geol. 412, 82-91.

Zhang, S., Jiang, G., Zhang, J., Song, B., Kennedy, M.J., Christie-Blick, N., 2005. U-Pb sensitive high-resolution ion microprobe ages from the Doushantuo Formation in south China: Constraints on late Neoproterozoic glaciations. Geology 33, 473-476.

Zhang, S., Jiang, G. and Han, Y., 2008. The age of the Nantuo Formation and Nantuo glaciation in South China. Terra Nova. 20, 289-294.

Zhang, X., Cui, L., 2016. Oxygen requirements for the Cambrian explosion. J. Earth. Sci-China. 27, 187-195.

Zhao, Y.-Y., Zheng, Y.-F., 2010. Stable isotope evidence for involvement of deglacial meltwater in Ediacaran carbonates in South China. Chem. Geol. 271, 86-100.

Zhao, Y.-Y., Zheng, Y.-F., Chen, F., 2009. Trace element and strontium isotope constraints on sedimentary environment of Ediacaran carbonates in southern Anhui, South China. Chem. Geol. 265, 345-362.

Zhao, Y.-Y., Zhao, M.Y., Li, S.Z., 2018. Evidences of hydrothermal fluids recorded in microfacies of the Ediacaran cap dolostone: Geochemical implications in South China. Precambrian. Res. 306, 1-21.

Zhu, M., Lu, M., Zhang, J., Zhao, F., Li, G., Yang, A., Zhao, X., Zhao, M., 2013. Carbon isotope chemostratigraphy and sedimentary facies evolution of the Ediacaran Doushantuo Formation in western Hubei, South China. Precambrian. Res. 225, 7-28.

Zhu, M., Zhang, J., Yang, A., 2007. Integrated Ediacaran (Sinian) chronostratigraphy of South China. Palaeogeogr. Palaeoclimatol. Palaeoecol. 254, 7-61.

Zhu, M., Zhang, J., Yang, A., Li, G., Steiner, M., Erdtmann, B.D., 2003. Sinian-Cambrian stratigraphic framework for shallow-to deep-water environments of the Yangtze Platform: an integrated approach. Prog. Nat. Sci. 13, 951-960.

Table captions

Table 1

Concentrations of major and trace elements and relevant calculated ratios in the three cap carboante section from Three Gorges area, South China. (a) Jiulongwan section; (b) Huajipo section; (c) Wuhe section. Grey asterisk labeled samples represent excluded points that may suffer diagenetic effects.

Table 2

Concentrations of REE and Y (ppm) and relevant calculated results in the three cap carbonate sections from Three Gorges area, South China. (a) Jiulongwan section; (b) Huajipo section; (c) Wuhe section. Grey asterisk labeled samples represent excluded points that may suffer diagenetic effect.

Figure captions

Fig. 1.

Simplified geological map of South China with the locations of the studied sections in both the Yangtze Platform and the basin, and a simplified shelf-to-basin transect from north to south in the Three Gorges area. (a) Generalized palaeogeographical reconstruction map of Chinese Ediacaran Yangtze Platform including the Three Gorges area. (b) Geological sketch map of the Three Gorges area in Hubei Province and the sampling sites. The study sections are marked with pentagrams. Modified after (Lu et al., 2013; Tian et al., 2014). (c) A conceptual transect across the Yangtze Block showing the stratigraphic occurrence of the Doushantuo cap carbonates. Modified after Jiang et al. (2003). Age data are cited from Condon et al. (2005) and Zhang et al. (2008).

Fig. 2.

PAAS-normalized Ce/Ce^*, total REE and Y/Ho ratios values of the three cap carbonate sections from Three Gorges area in South China. Red dashed lines represent $Ce/Ce^*>1.3$ (positive Ce anomalies), grey dashed lines display $Ce/Ce^*=1.0$, while black dashed lines present $Ce/Ce^*<0.9$ (negative Ce anomalies).

Fig. 3.

PAAS-normalized REE+Y patterns of unaltered cap carbonates in the three studied sections. (a-c) Samples from Jiulongwan cap carbonates. CA1 unit (below 1.25 m), CA2 unit (1.25-4.25m), CA3 unit (4.35-6.35m); (d-f) Samples from Huajipo cap carbonates. CA1 unit (below1.05m), CA2 unit (1.05-2.65m), CA3 unit (2.65-4.35m); (h-i) Samples from Wuhe cap carbonates. CA1 unit (below 1.20m), CA2 unit (1.20-2.2m), CA3 unit (2.20-4.8m).

Fig. 4.

Ce anomalies against trace element and major element influenced by terrestrial matters for assessing data quality. Key threshold values are highlighted by dashed lines. Threshold of Al/Ca< 8 is indicative of samples without terrestrial matters influence. Threshold of Y/Ho> 36 represents sample with seawater signature.

Fig. 5.

Plots of $\delta^{18}O$, $\delta^{13}C$ versus Mn/Sr to excluding diagenetic effects, together with Ce anomalies against trace elements and major elements influenced by hydrothermal and diagenetic processes for assessing data quality. Key threshold values are highlighted by dashed lines. Threshold of $\delta^{18}O$>-10‰ and Mn/Sr< 62 represent samples without diagenetic alteration, while bars of Eu/Eu^{*}>2 along with Ba/Nd> 100 may indicate the samples suffer later hydrothermal fluids alteration.

Fig. 6.

Comparison diagram of Ce anomalies in cap carbonates from previous work (Ling et al., 2013; Wang et al., 2014; Hu et al., 2016) and our study, and previous Fe species data from Jiulongwan cap carbonate section cited from Li et al. (2010).

Fig.7.

(a) Marine Fe-Mn (oxyhydr) oxide precipitates in plot of Ce/Ce* vs Nd concentration. (b) Marine Fe-Mn (oxyhydr) oxide precipitates in plot of Ce/Ce* vs Y/Y*values. The mean values of end-members are cited from (Alibo and Nozaki, 1999; Bau et al., 2014). Black bars represent mixing percentage between seawater and hydrogenetic Fe-Mn nodules. (c) Bivariate diagram of Ce/Ce* versus MREE/MREE* values in cap carbonate sections. Positive Ce anomalies outliers show unconpicuous MREE/MREE* ratios. (d) Bivariate diagram of Ce/Ce* versus Mn/Fe ratios in cap carbonate sections. Positive Ce anomalies outliers display distinct higher Mn/Fe ratios relative to other data points.

Fig. 8.

Schematic representation of redox zones and geochemical signals for the deposition of cap carbonates in the Three Gorges area. Modified after (Tostevin et al., 2016b; Yu et al., 2016). An anoxic ferruginous deep water mass is prevalent, while there is a sandwiched manganous wedge that represents extreme dysoxic condition with lower oxygen concentrations. Positive Ce anomalies form when Mn-(oxyhydr) oxides reductive dissolve in the manganous zone, excess oxide bound REY as $LnOH^{2+}$ release to ambient water simultaneously. The cap carbonates precipitate with freshwater joined that was melting from ice sheet under ultragreen house effect. Negative Ce anomalies display in well oxygenated zone. Submarine hydrothermal sources may supply numerous Fe and Mn ions and result in the positive Eu anomalies in REY patterns of cap carbonates. Category of redox condition associated with oceanic dissolved O_2 (DO) corresponds to early metazoan evolution. The mortality of benthic animals starts at DO below 45μM and massive mortality occurs at DO below 22.5μM (Tyson and Pearson, 1991; Diaz and Rosenberg, 1995).

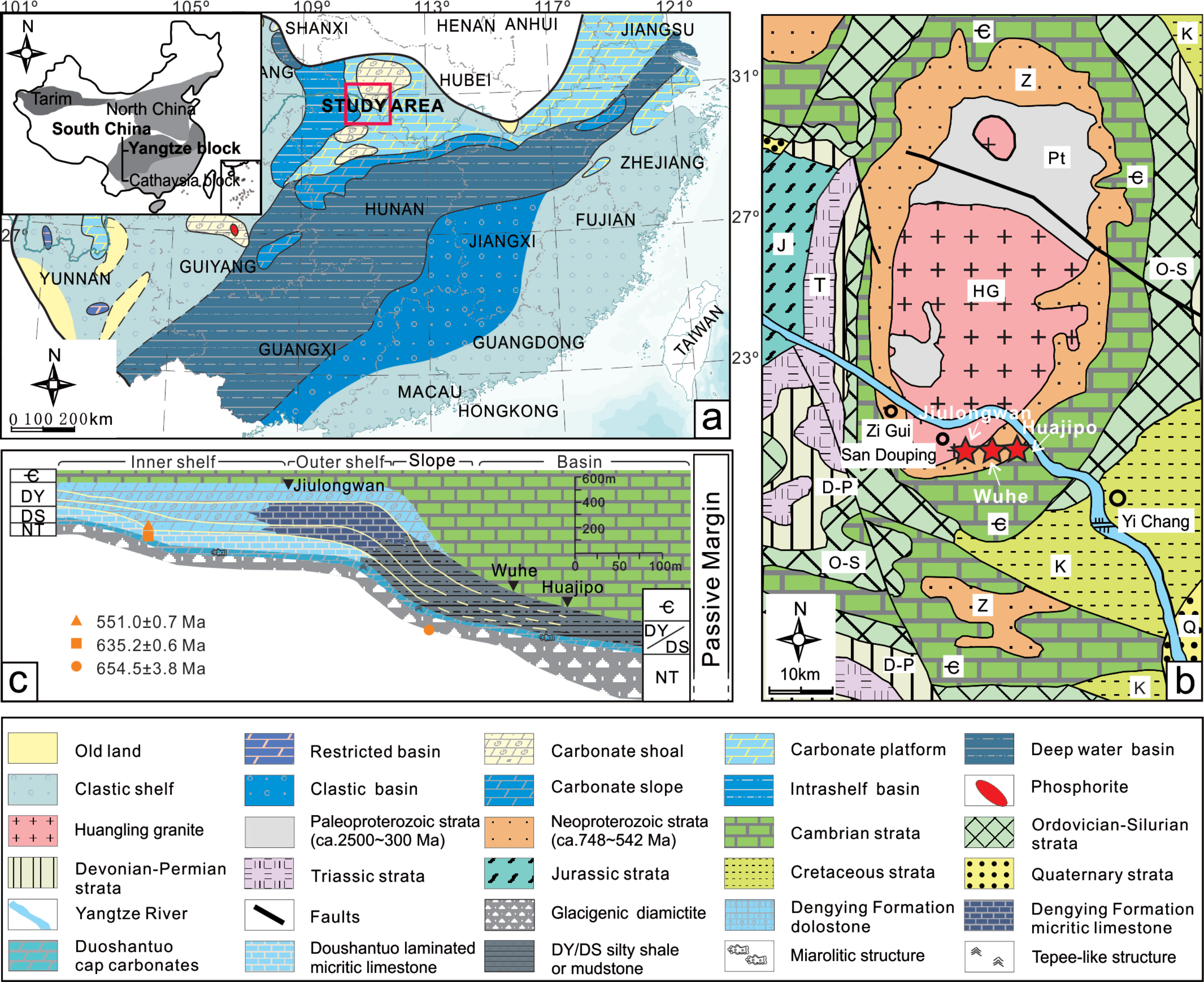

101°
105°
109°
113°
117°
121°
N
Tarim
North China
South China
Yangtze block
Cathaysia block
SHANXI
HENAN
ANHUI
JIANGSU
HUBEI
STUDY AREA
ZHEJIANG
HUNAN
FUJIAN
JIANGXI
GUIYANG
YUNNAN
GUANGXI
GUANGDONG
TAIWAN
MACAU
HONGKONG
31°
27°
23°
0 100 200km
a
Є
Z
K
Pt
Є
HG
J
T
O-S
Jiulongwan
Huajipo
Zi Gui
San Douping
Wuhe
D-P
Є
Yi Chang
O-S
K
Z
Q
N
10km
D-P
Є
K
b
Inner shelf
Outer shelf
Slope
Basin
Є
DY
DS
NT
Jiulongwan
600m
400
200
0
50
100m
Wuhe
Huajipo
Є
DY/DS
NT
Passive Margin
551.0±0.7 Ma
635.2±0.6 Ma
654.5±3.8 Ma
c
Old land
Restricted basin
Carbonate shoal
Carbonate platform
Deep water basin
Clastic shelf
Clastic basin
Carbonate slope
Intrashelf basin
Phosphorite
Huangling granite
Paleoproterozoic strata (ca.2500~300 Ma)
Neoproterozoic strata (ca.748~542 Ma)
Cambrian strata
Ordovician-Silurian strata
Devonian-Permian strata
Triassic strata
Jurassic strata
Cretaceous strata
Quaternary strata
Yangtze River
Faults
Glacigenic diamictite
Dengying Formation dolostone
Dengying Formation micritic limestone
Duoshantuo cap carbonates
Doushantuo laminated micritic limestone
DY/DS silty shale or mudstone
Miarolitic structure
Tepee-like structure

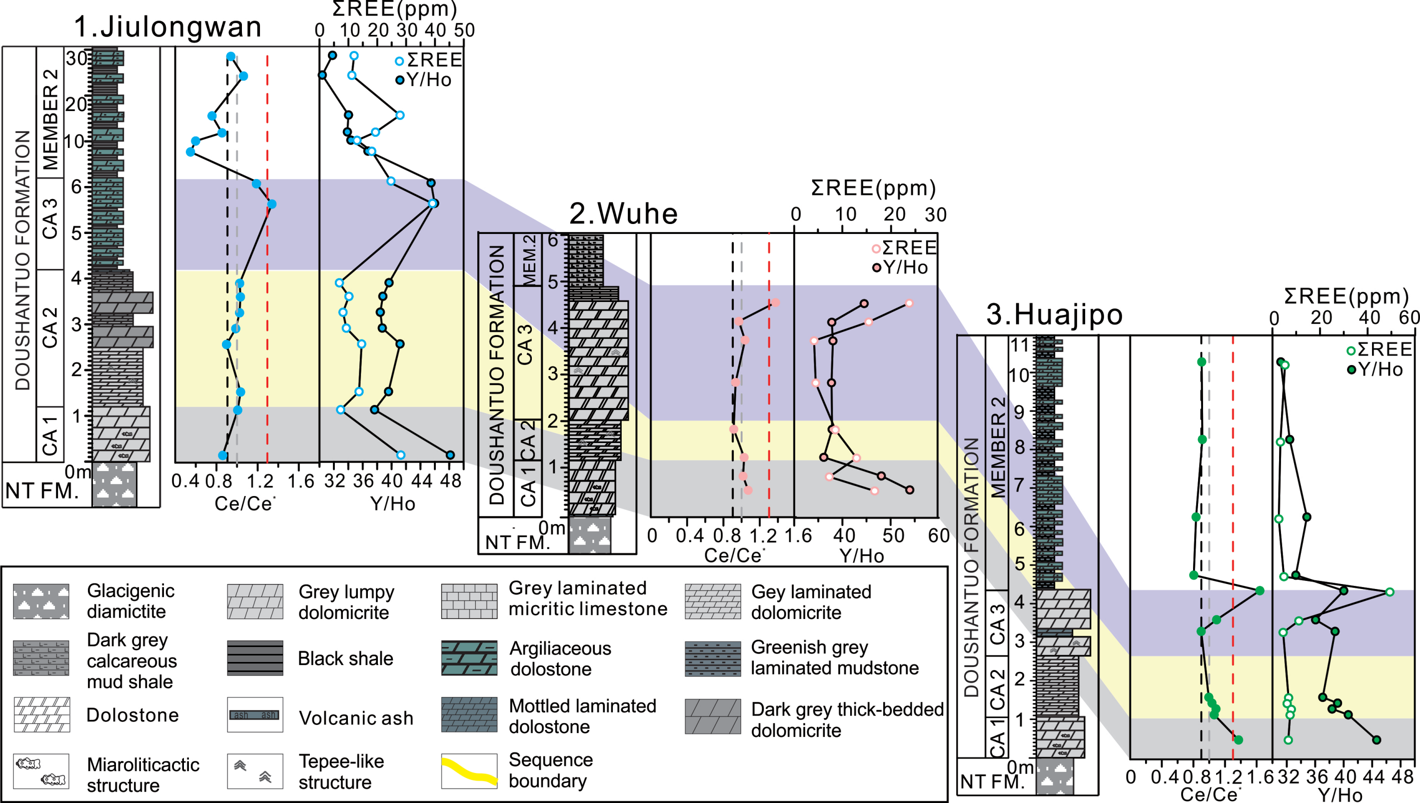
1.Jiulongwan
2.Wuhe
3.Huajipo
ΣREE(ppm)
ΣREE
Y/Ho
Ce/Ce*
DOUSHANTUO FORMATION
MEMBER 2
MEM.2
CA 3
CA 2
CA 1
NT FM.
0m
Glacigenic diamictite
Grey lumpy dolomicrite
Grey laminated micritic limestone
Gey laminated dolomicrite
Dark grey calcareous mud shale
Black shale
Argiliaceous dolostone
Greenish grey laminated mudstone
Dolostone
Volcanic ash
Mottled laminated dolostone
Dark grey thick-bedded dolomicrite
Miaroliticactic structure
Tepee-like structure
Sequence boundary

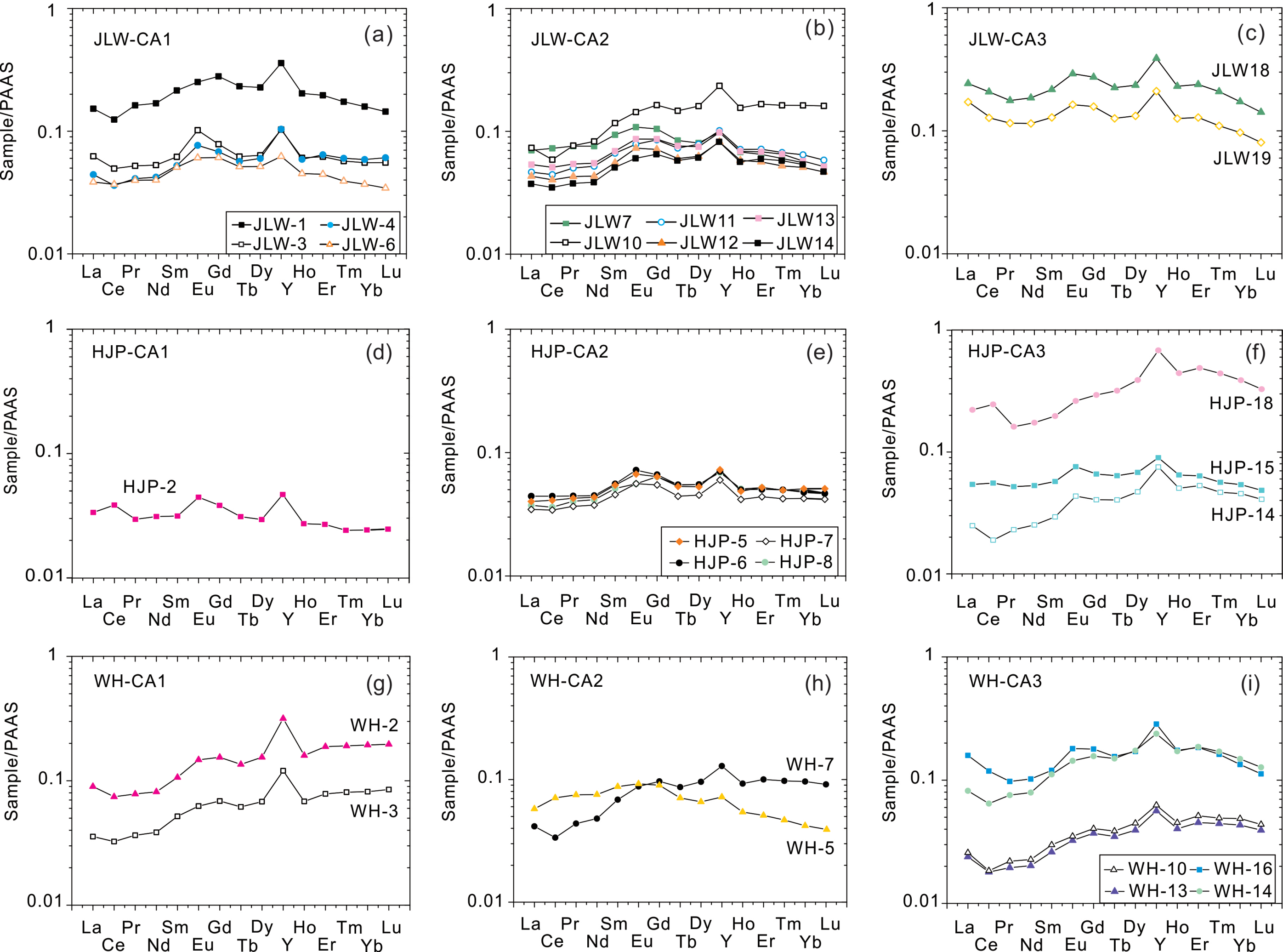

JLW-CA1
(a)
JLW-1
JLW-3
JLW-4
JLW-6
JLW-CA2
(b)
JLW7
JLW10
JLW11
JLW12
JLW13
JLW14
JLW-CA3
(c)
JLW18
JLW19
HJP-CA1
(d)
HJP-2
HJP-CA2
(e)
HJP-5
HJP-6
HJP-7
HJP-8
HJP-CA3
(f)
HJP-18
HJP-15
HJP-14
WH-CA1
(g)
WH-2
WH-3
WH-CA2
(h)
WH-7
WH-5
WH-CA3
(i)
WH-10
WH-13
WH-16
WH-14
Sample/PAAS
1
0.1
0.01
La
Ce
Pr
Nd
Sm
Eu
Gd
Tb
Dy
Y
Ho
Er
Tm
Yb
Lu

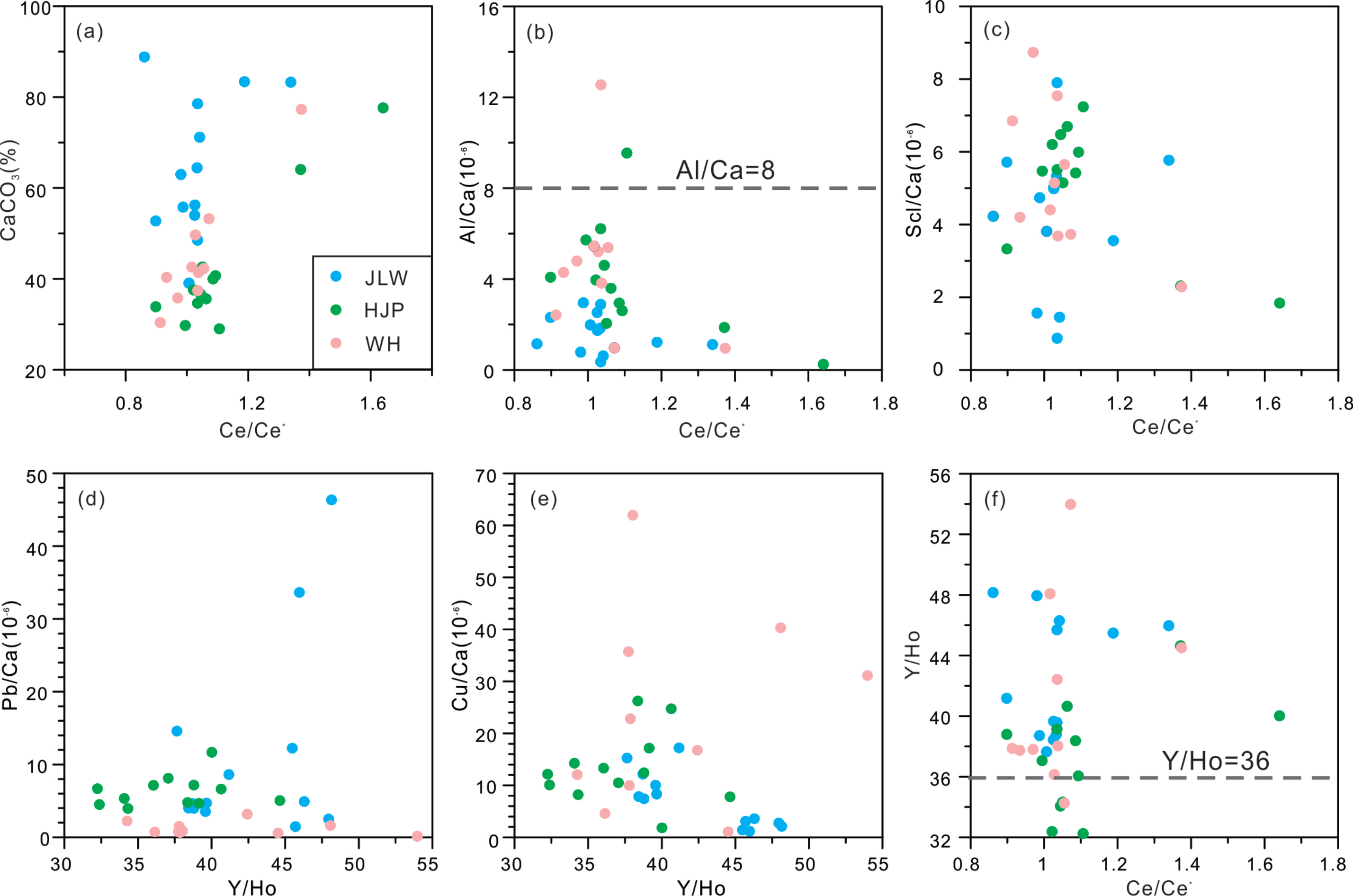

(a)
(b)
(c)
(d)
(e)
(f)
JLW
HJP
WH
Al/Ca=8
Y/Ho=36
$CaCO_3$(%)
Al/Ca(10^{-6})
ScI/Ca(10^{-6})
Pb/Ca(10^{-6})
Cu/Ca(10^{-6})
Y/Ho
Ce/Ce*
Y/Ho

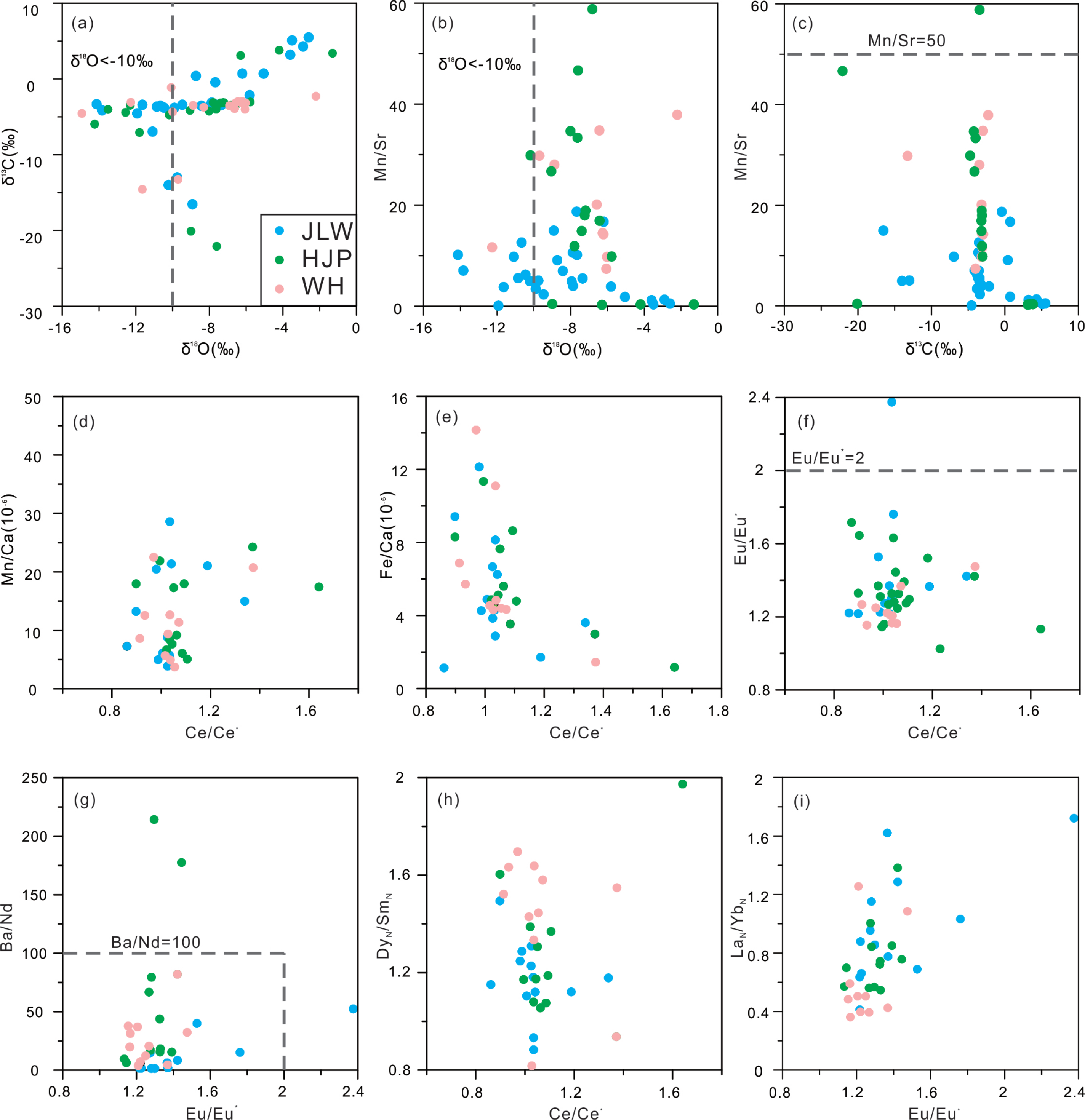
(a)
δ18O<-10‰
δ13C(‰)
δ18O(‰)
JLW
HJP
WH
(b)
δ18O<-10‰
Mn/Sr
δ18O(‰)
(c)
Mn/Sr=50
Mn/Sr
δ13C(‰)
(d)
Mn/Ca(10-6)
Ce/Ce*
(e)
Fe/Ca(10-6)
Ce/Ce*
(f)
Eu/Eu*=2
Eu/Eu*
Ce/Ce*
(g)
Ba/Nd=100
Ba/Nd
Eu/Eu*
(h)
DyN/SmN
Ce/Ce*
(i)
LaN/YbN
Eu/Eu*

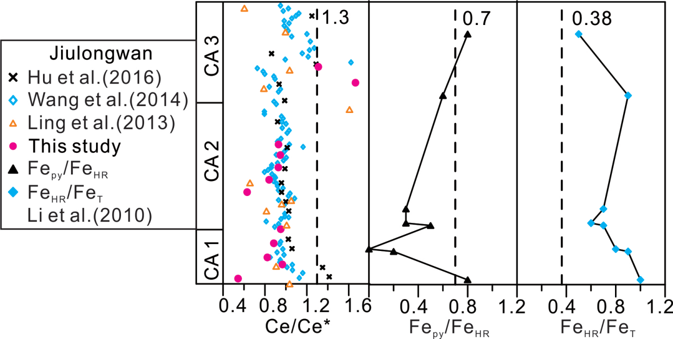

Jiulongwan
Hu et al.(2016)
Wang et al.(2014)
Ling et al.(2013)
This study
Fe_{py}/Fe_{HR}
Fe_{HR}/Fe_T
Li et al.(2010)
CA 3
CA 2
CA 1
1.3
0.7
0.38
0.4 0.8 1.2 1.6
Ce/Ce*
0.4 0.8 1.2
Fe_{py}/Fe_{HR}
0.4 0.8 1.2
Fe_{HR}/Fe_T

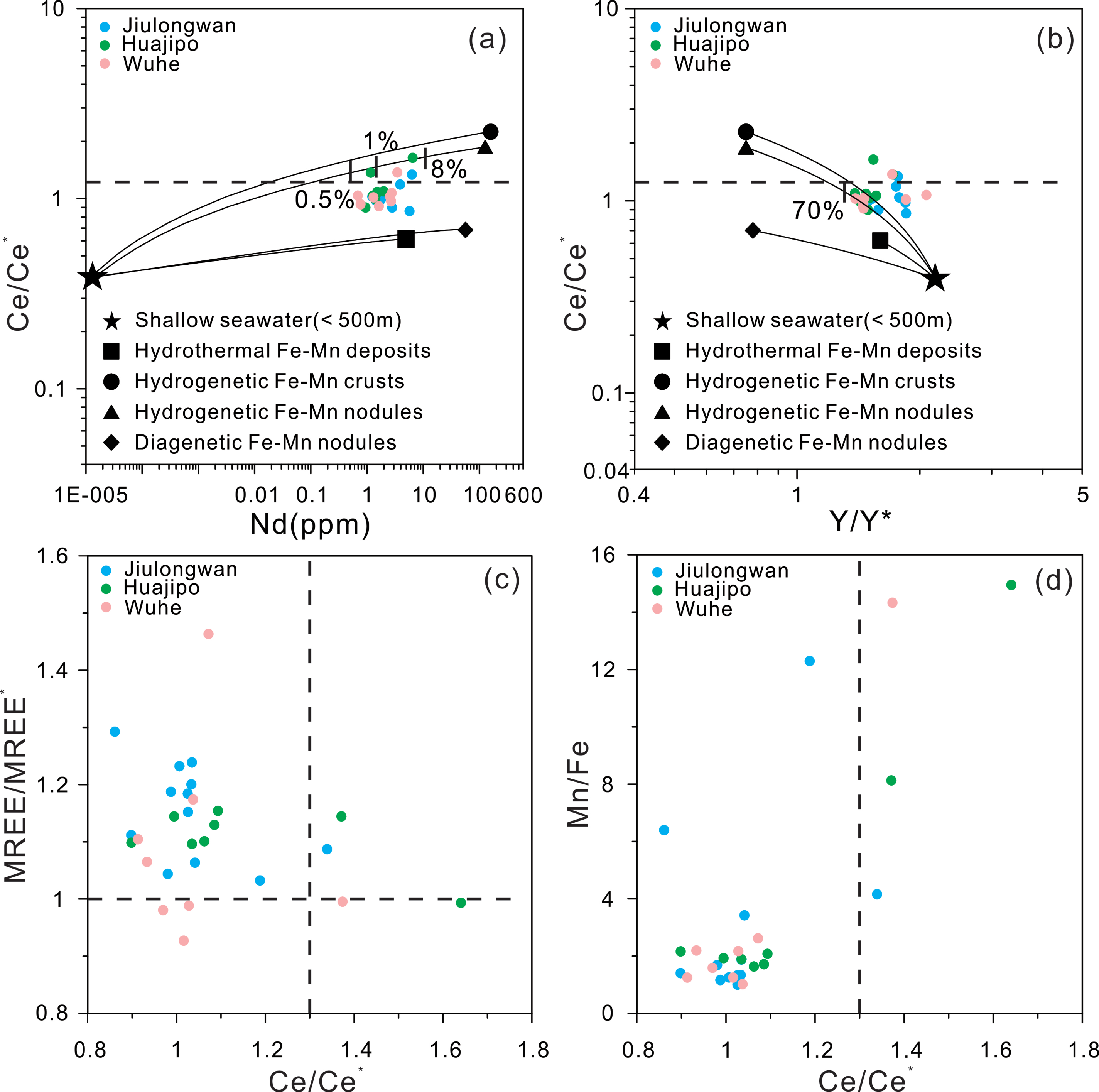

(a)
Jiulongwan
Huajipo
Wuhe
1%
8%
0.5%
Shallow seawater(< 500m)
Hydrothermal Fe-Mn deposits
Hydrogenetic Fe-Mn crusts
Hydrogenetic Fe-Mn nodules
Diagenetic Fe-Mn nodules
Ce/Ce*
Nd(ppm)
(b)
70%
Y/Y*
(c)
MREE/MREE*
Ce/Ce*
(d)
Mn/Fe
Ce/Ce*

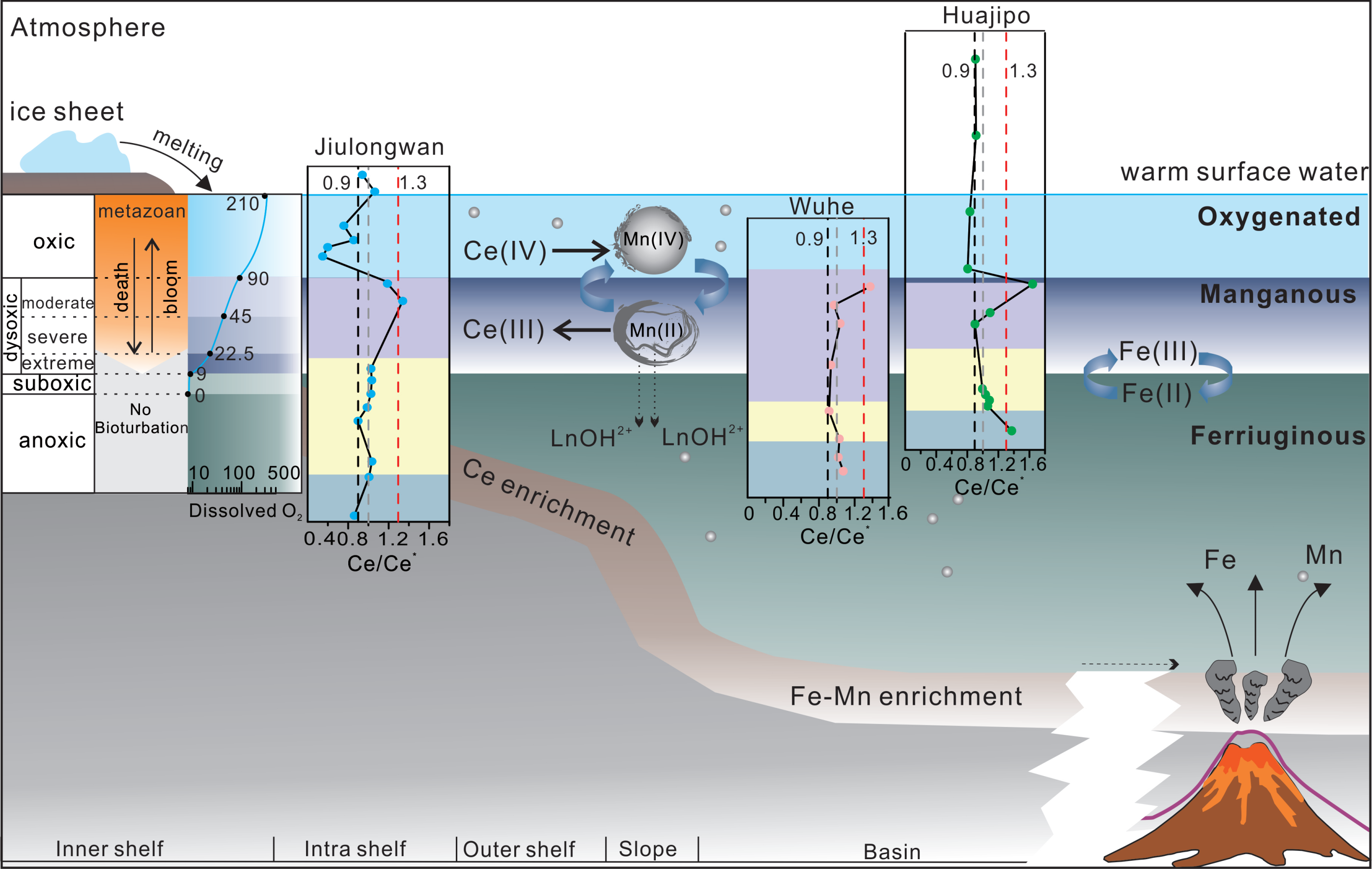

Atmosphere
ice sheet
melting
Jiulongwan
Huajipo
Wuhe
warm surface water
Oxygenated
Manganous
Ferriuginous
oxic
dysoxic
moderate
severe
extreme
suboxic
anoxic
metazoan
death
bloom
No Bioturbation
210
90
45
22.5
9
0
10 100 500
Dissolved O_2
0.9
1.3
0.4 0.8 1.2 1.6
0 0.4 0.8 1.2 1.6
Ce/Ce^*
Ce(IV)
Ce(III)
Mn(IV)
Mn(II)
$LnOH^{2+}$
Fe(III)
Fe(II)
Ce enrichment
Fe-Mn enrichment
Fe
Mn
Inner shelf
Intra shelf
Outer shelf
Slope
Basin

(a) Jiulongwan section, the Three Gorges area, South China

Samples	Member	Depth	Ca	Mg	Mn	Fe	Al	Ba	Pb	Cu	Sc	Co	Sr	$\delta^{13}C_{PDB}$	$\delta^{18}O_{PDB}$	$CaCO_3$	Mn/Fe	Mn/Sr	Co/Ca
		(m)	(wt%)	(wt%)	(wt%)	(wt%)	(wt%)	(ppm)	(ppm)	(ppm)	(ppm)	(ppm)	(ppm)	(‰)	(‰)	(%)			(10^{-6})
JLW-1	CA1	0.15	35.50	0.03	0.06	0.01	0.04	35.8	16.47	0.75	1.50	0.69	70.94	0.40	-8.73	83.38	6.40	9.09	1.94
JLW-2*	CA1	0.35	31.40	1.20	0.23	0.07	0.01	102.78	0.46	0.97	0.27	0.26	227.31	-3.33	-14.13	83.27	3.51	10.15	0.83
JLW-3	CA1	0.55	28.50	0.95	0.15	0.04	0.02	27.28	1.40	1.02	0.41	0.25	216.15	-4.14	-13.84	88.02	3.42	7.03	0.89
JLW-4	CA1	0.75	25.20	0.98	0.13	0.08	0.02	57.25	0.63	0.70	0.39	0.22	132.47	-6.95	-11.09	61.42	1.69	9.75	0.87
JLW-5*	CA1	0.95	30.90	0.53	0.12	0.02	0.05	60.11	2.28	1.23	0.82	0.60	320.37	-3.41	-11.64	83.27	5.14	3.76	1.95
JLW-6	CA1	1.15	15.60	1.91	0.02	0.02	0.03	20.07	2.28	2.38	0.60	1.07	62.17	-2.14	-5.81	56.24	1.25	3.87	6.87
JLW-7	CA2	1.55	19.40	1.31	0.02	0.01	0.06	3.77	0.69	1.95	1.53	0.76	102.4	-3.41	-9.47	64.43	1.88	2.31	3.92
JLW-8*	CA2	1.90	21.20	1.84	0.04	0.03	0.05	3.61	1.63	3.38	1.09	1.22	71.77	-3.66	-10.86	54.00	1.42	5.53	5.75
JLW-9*	CA2	2.25	18.60	1.95	0.08	0.05	0.04	7.51	1.94	3.20	1.08	1.14	62.56	-3.54	-10.67	55.78	1.45	12.59	6.13
JLW-10	CA2	2.60	21.10	1.86	0.07	0.05	0.05	4.61	1.82	3.63	1.21	1.35	68.49	-3.40	-7.66	52.74	1.41	10.13	6.42
JLW-11	CA2	2.95	22.30	1.91	0.03	0.02	0.07	2.99	1.03	2.71	1.06	1.06	56.86	-3.46	-7.95	46.56	1.16	4.89	4.75
JLW-12	CA2	3.30	21.60	2.53	0.05	0.04	0.05	3.01	0.86	1.69	1.08	1.08	70.13	-3.54	-8.43	52.9	1.32	6.95	5.01
JLW-13	CA2	3.65	25.80	2.07	0.04	0.03	0.05	2.73	1.02	1.91	1.37	1.49	70.76	-3.45	-7.35	48.52	1.34	5.48	5.79
JLW-14	CA2	3.95	22.50	2.45	0.02	0.02	0.04	2.47	1.06	1.87	1.12	1.04	64.13	-3.81	-9.90	39.06	1.00	3.41	4.63
JLW-15*	CA3	4.35	33.30	2.20	0.09	0.06	0.02	52.67	1.31	9.4	0.89	1.22	144.24	-3.79	-10.46	77.25	1.44	6.23	3.66
JLW-16*	CA3	4.80	55.00	0.09	0.00	0.02	0.02	37.51	1.33	4.05	1.66	0.83	232.43	-4.55	-11.93	62.97	0.07	0.07	1.51
JLW-17*	CA3	5.25	35.20	1.53	0.09	0.05	0.02	32.2	2.20	3.54	0.70	1.05	185.36	-14.00	-10.22	71.17	1.91	4.95	2.97
JLW-18	CA3	5.70	33.30	0.58	0.12	0.03	0.04	52.85	11.2	0.39	1.92	1.89	247.59	-13.00	-9.75	78.54	4.16	5.04	5.66
JLW-19	CA3	6.15	33.40	0.65	0.17	0.01	0.04	24.36	4.08	0.47	1.19	1.95	115.02	-16.54	-8.92	88.83	12.30	14.95	5.84
JLW-24	Mem2	11.60	12.20	4.70	0.18	0.14	0.18	28.63	1.23	1.01	0.18	0.38	130.90	-3.12	-7.87	30.61	1.29	13.90	3.11
JLW-25	Mem2	13.60	12.20	7.80	0.19	0.24	0.35	91.57	1.12	2.33	0.28	0.68	347.52	0.71	-5.05	30.43	0.83	5.61	5.57

JLW-27	Mem2	**15.10**	**9.30**	**4.30**	**0.04**	**0.13**	**0.04**	**81.92**	**0.39**	**0.22**	**2.34**	**0.82**	**306.62**	**3.20**	**-3.60**	**23.15**	**0.27**	**1.16**	**8.82**
JLW-31	Mem2	**18.20**	**9.10**	**4.00**	**0.04**	**0.14**	**0.06**	**55.79**	**0.29**	**0.19**	**2.76**	**0.70**	**277.91**	**4.30**	**-2.90**	**22.64**	**0.25**	**1.28**	**7.69**
JLW-33	Mem2	**25.50**	**11.10**	**5.00**	**0.03**	**0.10**	**0.03**	**359.77**	**0.23**	**0.29**	**1.89**	**0.61**	**591.92**	**5.50**	**-2.60**	**27.69**	**0.29**	**0.49**	**5.50**
JLW-35	Mem2	**29.10**	**8.90**	**4.60**	**0.02**	**0.19**	**0.05**	**301.52**	**0.22**	**1.42**	**2.76**	**1.81**	**636.37**	**5.10**	**-3.50**	**22.27**	**0.12**	**0.35**	**20.34**

(b) Huajipo section, the Three Gorges area, South China

Samples	**Member**	**Depth**	**Ca**	**Mg**	**Mn**	**Fe**	**Al**	**Ba**	**Pb**	**Cu**	**Sc**	**Co**	**Sr**	**$\delta^{13}C_{PDB}$**	**$\delta^{18}O_{PDB}$**	**$CaCO_3$**	**Mn/Fe**	**Mn/Sr**	**Co/Ca**
		(m)	**(wt%)**	**(wt%)**	**(wt%)**	**(wt%)**	**(wt%)**	**(ppm)**	**(ppm)**	**(ppm)**	**(ppm)**	**(ppm)**	**(ppm)**	**(‰)**	**(‰)**	**(%)**			**(10^{-6})**
HJP-1*	CA1	**0.25**	24.20	0.40	0.97	0.24	0.14	88.73	6.18	0.84	3.02	1.55	261.86	−6.00	−14.20	19.08	4.10	36.86	6.41
HJP-2	CA1	**0.50**	25.60	2.90	0.62	0.08	0.05	95.5	1.29	2.00	0.59	1.00	208.23	−4.70	−10.20	17.98	8.13	29.85	3.90
HJP-3*	CA1	**0.75**	26.40	1.90	0.28	0.05	0.06	18.45	0.74	1.75	0.77	0.51	207.72	−3.50	−12.30	17.90	5.06	13.30	1.92
HJP-4*	CA1	**1.00**	34.40	1.00	0.61	0.07	0.05	63.08	1.13	2.00	0.84	1.02	209.76	−4.00	−13.50	20.80	8.99	28.86	2.96
HJP-5	CA2	**1.15**	14.20	6.20	0.13	0.08	0.05	64.67	0.94	3.52	0.95	1.12	72.78	−3.10	−7.20	77.64	1.64	17.96	7.89
HJP-6	CA2	**1.30**	16.00	6.70	0.10	0.06	0.05	23.53	0.76	4.20	0.87	0.72	81.86	−3.10	−7.80	60.99	1.72	11.87	4.50
HJP-7	CA2	**1.45**	13.90	5.90	0.12	0.06	0.09	19.86	0.65	2.38	0.76	0.79	61.43	−3.20	−7.20	40.71	1.89	18.91	5.72
HJP-8	CA2	**1.60**	11.90	5.60	0.26	0.13	0.07	8.91	0.96	1.25	0.65	0.89	44.28	−3.50	−6.80	33.87	1.93	58.81	7.44
HJP-9*	CA2	**1.90**	14.70	6.60	0.11	0.08	0.07	129.15	0.78	2.09	0.95	0.96	75.49	−3.20	−7.40	57.19	1.49	14.86	6.52
HJP-10*	CA2	**1.95**	11.60	6.70	0.06	0.06	0.11	164.76	0.77	1.41	0.84	1.03	59.99	−3.00	−5.80	42.60	1.06	9.82	8.91
HJP-11*	CA2	**2.05**	15.00	7.80	0.10	0.07	0.06	59.66	0.68	1.51	0.93	0.74	59.31	−3.20	−6.40	37.57	1.37	16.90	4.92
HJP-12*	CA2	**2.25**	17.00	6.00	0.29	0.13	0.03	147.28	0.67	1.40	0.88	0.67	110.44	−4.10	−9.10	29.01	2.26	26.70	3.92
HJP-13*	CA3	**3.05**	22.90	2.70	0.25	0.06	0.06	4.21	0.51	0.66	1.14	0.37	115.85	−4.40	−12.60	36.67	4.22	22.00	1.62
HJP-14	CA3	**3.30**	13.50	6.50	0.24	0.11	0.06	17.22	0.97	1.68	0.45	0.50	72.96	−4.00	−7.60	29.75	2.16	33.35	3.71
HJP-15	CA3	**3.60**	16.30	6.20	0.29	0.14	0.04	33.48	1.16	2.17	0.98	0.92	84.42	−4.20	−8.00	34.66	2.08	34.65	5.62
HJP-16*	CA3	**4.20**	24.40	1.40	0.36	0.06	0.05	89.88	18.81	1.61	0.80	7.00	121.29	−7.10	−11.80	40.00	6.35	29.27	28.71
HJP-18	CA3	**4.35**	31.10	1.10	0.54	0.04	0.01	62.06	3.63	0.57	0.57	1.64	116.00	−22.10	7.60	35.61	14.95	46.67	5.28

HJP-20	Mem.2	**4.75**	8.30	4.40	0.01	0.20	0.02	199.82	0.07	0.83	1.04	0.44	351.41	−20.10	−9.00	85.92	0.07	0.40	5.33
HJP-22	Mem.2	**6.25**	7.20	3.80	0.01	0.14	0.02	218.72	0.12	0.94	0.86	0.47	386.48	3.10	−6.30	66.08	0.07	0.24	6.58
HJP-24	Mem.2	**8.25**	7.20	4.00	0.01	0.11	0.02	129.09	0.06	0.74	1.18	0.07	366.63	3.40	−1.30	64.06	0.11	0.33	1.00
HJP-26	Mem.2	**10.25**	7.60	4.50	0.01	0.10	0.03	166.41	0.11	1.03	1.37	1.96	381.35	3.80	−4.20	60.48	0.13	0.33	25.74

(c) Wuhe section, the Three Gorges area, South China

Samples	**Member**	**Depth**	**Ca**	**Mg**	**Mn**	**Fe**	**Al**	**Ba**	**Pb**	**Cu**	**Sc**	**Co**	**Sr**	**$\delta^{13}C_{PDB}$**	**$\delta^{18}O_{PDB}$**	**$CaCO_3$**	**Mn/Fe**	**Mn/Sr**	**Co/Ca**
		(m)	**(wt%)**	**(wt%)**	**(wt%)**	**(wt%)**	**(wt%)**	**(ppm)**	**(ppm)**	**(ppm)**	**(ppm)**	**(ppm)**	**(ppm)**	**(‰)**	**(‰)**	**(%)**			**(10^{-6})**
WH-1*	CA1	**0.10**	31.50	0.50	0.57	0.11	0.04	93.68	2.10	0.96	1.18	0.79	347.08	−4.55	−14.93	37.76	5.44	16.54	2.52
WH-2	CA1	**0.60**	21.30	3.90	0.24	0.09	0.02	12.69	1.59	6.63	0.79	0.79	207.97	−3.09	−12.27	77.30	2.62	11.63	3.70
WH-3	CA1	**0.90**	17.00	9.20	0.10	0.08	0.09	9.50	1.86	6.87	0.75	4.64	68.18	−2.96	−6.22	80.83	1.25	14.22	27.21
WH-4*	CA1	**1.10**	15.00	8.30	0.19	0.17	0.19	64.03	1.28	2.51	1.13	119.91	54.40	−2.98	−6.44	35.79	1.14	34.79	800.79
WH-5	CA2	**1.30**	19.90	7.00	0.19	0.09	0.10	10.03	0.69	0.91	1.02	1.82	92.72	−3.18	−6.58	41.38	2.17	20.10	9.17
WH-6*	CA2	**1.70**	16.00	8.40	0.39	0.23	0.10	31.12	1.57	1.37	1.09	7.83	60.18	−3.53	−6.91	57.52	1.70	64.45	49.06
WH-7	CA2	**1.90**	12.20	5.90	0.10	0.08	0.03	33.55	1.46	2.77	0.83	0.88	72.18	−3.15	−6.26	37.87	1.25	14.47	7.21
WH-8*	CA3	**2.20**	12.50	5.90	0.51	0.23	0.03	106.78	0.54	0.84	0.84	0.64	62.57	−3.73	−8.31	40.34	2.21	82.29	5.10
WH-9*	CA3	**2.40**	16.90	9.50	0.06	0.07	0.09	18.72	1.82	2.04	0.95	2.07	64.67	−3.17	−6.03	42.26	0.85	9.73	12.25
WH-10	CA3	**2.90**	16.10	8.40	0.20	0.09	0.07	29.07	0.91	5.76	0.68	0.99	53.46	−2.28	−2.20	31.26	2.20	37.90	6.14
WH-11*	CA3	**3.20**	15.10	7.90	0.31	0.11	0.06	14.95	0.70	5.25	0.56	1.07	37.92	−3.91	−6.63	30.38	2.72	81.82	7.10
WH-12*	CA3	**3.50**	23.00	4.80	0.27	0.11	0.10	14.52	1.57	0.53	1.47	1.20	154.36	−4.34	−10.00	39.88	2.61	17.80	5.22
WH-13	CA3	**3.80**	16.60	8.40	0.08	0.08	0.06	25.43	2.22	10.26	0.61	2.78	110.78	−4.00	−6.06	49.65	1.02	7.38	16.80
WH-14	CA3	**4.20**	14.30	7.30	0.32	0.20	0.07	33.05	2.46	1.43	1.25	1.90	115.02	−3.49	−8.89	37.43	1.59	28.01	13.26
WH-15*	CA3	**4.40**	32.30	0.40	0.52	0.04	0.03	616.64	2.45	0.51	0.51	12.07	428.55	−14.58	−11.64	42.6	12.52	12.05	37.33
WH-16	CA3	**4.60**	30.90	1.30	0.64	0.04	0.03	111.98	2.33	0.33	0.71	5.68	215.09	−13.25	−9.70	53.23	14.33	29.79	18.37
WH-17*	CA3	**4.80**	15.10	7.30	0.09	0.12	0.13	15.62	2.92	0.30	1.67	4.17	77.49	−1.13	−10.07	78.79	0.75	11.46	27.62

(a) Jiulongwan section, the Three Gorges area, South China

Samples	Member	Depth	La	Ce	Pr	Nd	Sm	Eu	Gd	Tb	Dy	Y	Ho	Er	Tm	Yb	Lu	∑REE	Ce/Ce^*	Eu/Eu^*	Y/Ho	Y^*	Dy_n/Sm_n	Ba/Nd	La_n/Yb_n	$MREE/MREE^*$
		(m)	(ppm)	(ppm)	(ppm)	(ppm)	(ppm)	(ppm)	(ppm)	(ppm)	(ppm)	(ppm)	(ppm)	(ppm)	(ppm)	(ppm)	(ppm)	(ppm)								
JLW-1	CA1	0.15	5.82	9.90	1.43	5.71	1.19	0.27	1.30	0.18	1.06	9.69	0.20	0.56	0.07	0.45	0.06	28.21	0.86	1.22	48.15	1.86	1.15	6.27	0.88	1.29
JLW-2*	CA1	0.35	2.56	4.38	0.51	1.96	0.38	0.16	0.39	0.05	0.26	2.11	0.05	0.12	0.02	0.10	0.02	10.93	1.04	2.38	45.7	1.62	0.88	52.4	1.72	1.21
JLW-3	CA1	0.55	2.39	3.95	0.46	1.79	0.34	0.11	0.36	0.05	0.30	2.78	0.06	0.18	0.02	0.16	0.02	10.19	1.04	1.76	46.29	1.78	1.12	15.21	1.03	1.06
JLW-4	CA1	0.75	1.69	2.88	0.36	1.43	0.29	0.08	0.32	0.04	0.28	2.80	0.06	0.18	0.02	0.17	0.03	7.83	0.98	1.53	47.95	1.79	1.25	40.03	0.69	1.04
JLW-5*	CA1	0.95	4.00	7.12	0.82	3.24	0.64	0.24	0.68	0.08	0.41	2.77	0.07	0.17	0.02	0.12	0.02	17.63	1.06	2.13	40.16	1.52	0.83	18.54	2.17	1.37
JLW-6	CA1	1.15	1.47	2.93	0.35	1.35	0.28	0.07	0.28	0.04	0.24	1.68	0.04	0.13	0.02	0.10	0.01	7.33	1.01	1.27	37.64	1.61	1.10	14.81	0.95	1.23
JLW-7	CA2	1.55	2.67	5.78	0.67	2.56	0.52	0.12	0.49	0.07	0.38	2.66	0.07	0.18	0.02	0.16	0.02	13.71	1.04	1.28	39.58	1.46	0.93	1.47	1.15	1.24
JLW-8*	CA2	1.90	2.62	4.76	0.67	2.71	0.61	0.16	0.67	0.10	0.62	5.09	0.12	0.38	0.05	0.37	0.06	13.88	0.90	1.36	41.05	1.63	1.31	1.33	0.48	1.13
JLW-9*	CA2	2.25	2.16	3.98	0.57	2.38	0.54	0.13	0.62	0.09	0.6	4.91	0.12	0.38	0.05	0.36	0.05	12.03	0.91	1.23	40.12	1.57	1.43	3.16	0.41	1.13
JLW-10	CA2	2.60	2.80	4.67	0.68	2.81	0.65	0.15	0.76	0.11	0.75	6.34	0.15	0.48	0.07	0.46	0.07	14.61	0.90	1.22	41.17	1.63	1.49	1.64	0.41	1.11
JLW-11	CA2	2.95	1.78	3.53	0.44	1.76	0.37	0.08	0.4	0.06	0.37	2.73	0.07	0.2	0.03	0.18	0.03	9.30	0.99	1.23	38.71	1.50	1.29	1.70	0.66	1.19
JLW-12	CA2	3.30	1.65	3.21	0.38	1.46	0.31	0.08	0.33	0.05	0.29	2.21	0.06	0.16	0.02	0.14	0.02	8.16	1.03	1.37	38.44	1.42	1.23	2.05	0.78	1.18
JLW-13	CA2	3.65	2.05	4.05	0.48	1.87	0.38	0.09	0.4	0.06	0.35	2.64	0.07	0.19	0.03	0.16	0.02	10.21	1.03	1.30	38.79	1.45	1.18	1.47	0.86	1.20
JLW-14	CA2	3.95	1.36	2.64	0.32	1.24	0.27	0.06	0.29	0.04	0.27	2.11	0.05	0.16	0.02	0.14	0.02	6.89	1.03	1.22	39.65	1.62	1.31	1.99	0.64	1.15
JLW-15*	CA3	4.35	3.34	5.44	0.56	2.11	0.41	0.13	0.46	0.06	0.39	3.50	0.08	0.22	0.03	0.16	0.02	13.43	1.13	1.64	44.85	1.68	1.23	24.95	1.38	1.13
JLW-16*	CA3	4.80	7.69	13.39	1.52	5.39	0.95	0.18	0.90	0.13	0.80	5.75	0.15	0.44	0.06	0.38	0.05	32.04	0.98	1.04	37.48	1.47	1.09	6.96	1.35	1.01
JLW-17*	CA3	5.25	6.58	10.39	1.26	4.90	0.97	0.26	1.07	0.15	0.89	7.95	0.17	0.50	0.06	0.37	0.05	27.6	1.00	1.45	46.46	1.80	1.18	6.57	1.21	1.19
JLW-18	CA3	5.70	9.26	16.49	1.56	6.29	1.2	0.31	1.27	0.17	1.10	10.49	0.23	0.68	0.08	0.49	0.06	39.20	1.34	1.42	45.97	1.75	1.18	8.41	1.29	1.09
JLW-19	CA3	6.15	6.55	10.16	1.02	3.89	0.71	0.18	0.73	0.10	0.62	5.68	0.12	0.37	0.04	0.27	0.03	24.79	1.19	1.37	45.48	1.82	1.12	6.27	1.62	1.03
JLW-24	Mem2	11.60	5.98	5.40	1.10	3.90	0.53	0.12	0.37	0.09	0.27	1.94	0.05	0.12	0.05	0.11	0.02	18.11	0.55	1.19	36.73	1.49	0.66	7.33	3.55	0.83
JLW-25	Mem2	13.60	3.57	4.08	0.79	2.91	0.47	0.14	0.32	0.08	0.27	1.86	0.05	0.12	0.05	0.13	0.03	13.00	0.60	1.50	34.35	1.43	0.75	31.48	1.89	0.94

JLW-27	Mem2	15.10	5.10	6.97	0.99	3.84	0.70	0.20	0.62	0.08	0.42	2.50	0.07	0.20	0.03	0.16	0.02	19.42	0.85	1.67	33.87	1.37	0.78	21.34	2.01	1.14
JLW-31	Mem2	18.20	7.19	9.01	1.52	6.21	1.15	0.33	1.03	0.13	0.69	3.87	0.11	0.28	0.03	0.21	0.03	27.93	0.76	1.70	34.03	1.35	0.78	8.98	2.34	1.28
JLW-33	Mem2	25.50	2.50	4.41	0.52	2.08	0.42	0.13	0.40	0.05	0.32	1.70	0.06	0.16	0.02	0.13	0.02	11.22	1.06	1.72	30.4	1.09	0.97	172.78	1.28	1.23
JLW-35	Mem2	29.10	2.63	4.24	0.58	2.36	0.49	0.14	0.50	0.07	0.44	2.47	0.08	0.22	0.03	0.18	0.03	11.99	0.94	1.56	31.81	1.19	1.16	127.72	0.99	1.27

(b) Huajipo section, the Three Gorges area, South China

Samples		Depth	La	Ce	Pr	Nd	Sm	Eu	Gd	Tb	Dy	Y	Ho	Er	Tm	Yb	Lu	∑REE	Ce/Ce*	Eu/Eu*	Y/Ho	Y*	Dy_n/Sm_n	Ba/Nd	La_n/Yb_n	MREE/MREE*
		(m)	(ppm)	(ppm)	(ppm)	(ppm)	(ppm)	(ppm)	(ppm)	(ppm)	(ppm)	(ppm)	(ppm)	(ppm)	(ppm)	(ppm)	(ppm)	(ppm)								
HJP-1*	CA1	0.25	21.01	46.63	5.72	23.37	4.87	1.38	4.68	0.59	3.02	17.41	0.48	1.14	0.12	0.71	0.09	113.81	1.04	1.63	36.32	1.40	0.80	3.80	1.99	1.57
HJP-2	CA1	0.5	1.50	3.40	0.30	1.16	0.22	0.05	0.23	0.03	0.16	1.28	0.03	0.08	0.01	0.07	0.01	7.26	1.37	1.42	44.64	1.72	0.94	82.02	1.38	1.14
HJP-3*	CA1	0.75	1.58	3.13	0.32	1.23	0.24	0.07	0.26	0.04	0.22	2.17	0.05	0.14	0.02	0.13	0.02	7.43	1.18	1.52	48.07	1.85	1.19	14.99	0.82	1.02
HJP-4*	CA1	1.00	2.24	3.95	0.47	1.88	0.39	0.10	0.47	0.07	0.46	5.53	0.10	0.34	0.05	0.33	0.05	10.9	1.06	1.25	53.78	2.07	1.53	33.64	0.46	0.95
HJP-5	CA2	1.15	1.53	3.26	0.38	1.47	0.30	0.07	0.30	0.04	0.25	1.96	0.05	0.15	0.02	0.14	0.02	7.99	1.06	1.33	40.65	1.56	1.05	43.85	0.72	1.10
HJP-6	CA2	1.30	1.69	3.53	0.39	1.52	0.31	0.08	0.31	0.04	0.26	1.90	0.05	0.14	0.02	0.13	0.02	8.49	1.09	1.39	38.37	1.48	1.08	15.5	0.85	1.13
HJP-7	CA2	1.45	1.32	2.72	0.32	1.27	0.25	0.06	0.25	0.03	0.21	1.62	0.04	0.12	0.02	0.12	0.02	6.77	1.03	1.33	39.14	1.50	1.08	15.61	0.74	1.10
HJP-8	CA2	1.60	1.43	2.87	0.36	1.40	0.28	0.06	0.3	0.04	0.26	1.86	0.05	0.15	0.02	0.14	0.02	7.38	0.99	1.14	37.06	1.42	1.17	6.34	0.70	1.14
HJP-9*	CA2	1.90	1.76	3.55	0.42	1.63	0.33	0.08	0.33	0.05	0.30	1.93	0.06	0.16	0.02	0.14	0.02	8.82	1.04	1.28	34.07	1.31	1.17	79.46	0.84	1.16
HJP-10*	CA2	1.95	0.81	1.74	0.19	0.77	0.16	0.04	0.18	0.03	0.17	1.13	0.03	0.10	0.01	0.10	0.01	4.37	1.11	1.30	32.25	1.24	1.37	214.28	0.57	1.13
HJP-11*	CA2	2.05	0.95	1.96	0.23	0.89	0.19	0.04	0.19	0.03	0.20	1.29	0.04	0.12	0.02	0.11	0.02	4.99	1.02	1.27	32.38	1.24	1.39	66.74	0.56	1.07
HJP-12*	CA2	2.25	0.99	1.95	0.22	0.83	0.16	0.04	0.17	0.03	0.17	1.11	0.03	0.10	0.01	0.09	0.01	4.80	1.05	1.44	34.32	1.32	1.31	177.54	0.76	1.06
HJP-13*	CA3	3.05	3.81	7.22	0.85	3.24	0.61	0.13	0.62	0.09	0.55	4.24	0.11	0.30	0.04	0.23	0.03	17.85	1.00	1.16	39.65	1.52	1.17	1.30	1.11	1.15
HJP-14	CA3	3.30	1.11	1.67	0.23	0.94	0.20	0.05	0.24	0.04	0.25	2.06	0.05	0.16	0.02	0.14	0.02	5.13	0.90	1.33	38.79	1.49	1.60	18.31	0.55	1.10
HJP-15	CA3	3.60	2.41	4.90	0.53	1.98	0.39	0.09	0.40	0.06	0.36	2.45	0.07	0.20	0.03	0.16	0.02	11.59	1.09	1.28	36.05	1.39	1.19	16.93	1.00	1.15
HJP-16*	CA3	4.20	20.95	46.3	4.66	18.49	3.72	0.78	4.62	0.75	5.39	48.68	1.20	3.96	0.55	3.37	0.43	115.18	1.23	1.02	40.49	1.56	1.87	4.86	0.42	0.97
HJP-18	CA3	4.35	9.86	21.66	1.64	6.48	1.36	0.32	1.77	0.28	2.07	18.59	0.46	1.50	0.20	1.17	0.14	48.92	1.64	1.13	40.02	1.54	1.97	9.57	0.57	0.99

HJP-20	Mem.2	**4.75**	**1.27**	**1.86**	**0.27**	**1.08**	**0.21**	**0.07**	**0.20**	**0.03**	**0.2**	**1.27**	**0.04**	**0.11**	**0.01**	**0.09**	**0.01**	**5.46**	**0.87**	**1.72**	**33.28**	**1.28**	**1.23**	**184.5**	**0.92**	**1.10**
HJP-22	Mem.2	**6.25**	**0.71**	**1.10**	**0.16**	**0.68**	**0.14**	**0.04**	**0.15**	**0.02**	**0.14**	**0.98**	**0.03**	**0.09**	**0.01**	**0.07**	**0.01**	**3.37**	**0.90**	**1.65**	**34.83**	**1.34**	**1.30**	**323.01**	**0.69**	**1.17**
HJP-24	Mem.2	**8.25**	**0.74**	**1.44**	**0.19**	**0.81**	**0.18**	**0.04**	**0.19**	**0.03**	**0.18**	**1.07**	**0.03**	**0.09**	**0.01**	**0.08**	**0.01**	**4.03**	**0.99**	**1.31**	**32.42**	**1.25**	**1.24**	**159.73**	**0.63**	**1.31**
HJP-26	Mem.2	**10.25**	**1.08**	**1.98**	**0.27**	**1.17**	**0.28**	**0.07**	**0.31**	**0.05**	**0.30**	**1.80**	**0.06**	**0.17**	**0.02**	**0.14**	**0.02**	**5.91**	**0.98**	**1.37**	**31.17**	**1.20**	**1.38**	**141.77**	**0.53**	**1.29**

(c) Wuhe section, the Three Gorges area, South China

Samples		**Depth**	**La**	**Ce**	**Pr**	**Nd**	**Sm**	**Eu**	**Gd**	**Tb**	**Dy**	**Y**	**Ho**	**Er**	**Tm**	**Yb**	**Lu**	**∑REE**	**Ce/Ce***	**Eu/Eu***	**Y/Ho**	**Y***	**Dy_n/Sm_n**	**Ba/Nd**	**La_n/Yb_n**	**MREE/MREE***
		(m)	**(ppm)**	**(ppm)**	**(ppm)**	**(ppm)**	**(ppm)**	**(ppm)**	**(ppm)**	**(ppm)**	**(ppm)**	**(ppm)**	**(ppm)**	**(ppm)**	**(ppm)**	**(ppm)**	**(ppm)**	**(ppm)**								
WH-1*	CA1	0.10	14.01	28.70	3.31	13.44	2.75	0.88	2.73	0.33	1.76	11.59	0.29	0.73	0.08	0.47	0.06	69.55	1.10	1.84	39.42	1.52	0.83	6.97	2.03	1.46
WH-2	CA1	**0.60**	**3.44**	**5.92**	**0.69**	**2.76**	**0.59**	**0.16**	**0.72**	**0.10**	**0.72**	**8.54**	**0.16**	**0.54**	**0.08**	**0.55**	**0.09**	**16.51**	**1.07**	**1.37**	**53.97**	**2.08**	**1.58**	**4.60**	**0.42**	**0.93**
WH-3	CA1	**0.90**	**1.36**	**2.58**	**0.32**	**1.30**	**0.29**	**0.07**	**0.32**	**0.05**	**0.32**	**3.25**	**0.07**	**0.22**	**0.03**	**0.23**	**0.04**	**7.20**	**1.02**	**1.22**	**48.07**	**1.85**	**1.43**	**7.29**	**0.40**	**0.98**
WH-4*	CA1	1.10	1.82	4.16	0.51	2.04	0.45	0.10	0.47	0.07	0.46	4.14	0.10	0.32	0.05	0.34	0.05	10.94	1.04	1.17	42.42	1.63	1.33	31.37	0.36	0.99
WH-5	CA2	**1.30**	**2.21**	**5.65**	**0.66**	**2.56**	**0.49**	**0.10**	**0.42**	**0.05**	**0.31**	**1.95**	**0.05**	**0.15**	**0.02**	**0.12**	**0.02**	**12.79**	**1.03**	**1.21**	**36.14**	**1.39**	**0.82**	**3.92**	**1.26**	**1.24**
WH-6*	CA2	1.70	2.21	3.91	0.53	2.14	0.47	0.11	0.54	0.08	0.53	3.90	0.11	0.33	0.04	0.31	0.05	11.35	0.92	1.15	36.54	1.4	1.44	14.53	0.48	1.10
WH-7	CA2	**1.90**	**1.59**	**2.68**	**0.39**	**1.63**	**0.38**	**0.09**	**0.45**	**0.07**	**0.45**	**3.48**	**0.09**	**0.29**	**0.04**	**0.27**	**0.04**	**8.45**	**0.91**	**1.27**	**37.87**	**1.46**	**1.52**	**20.59**	**0.39**	**1.12**
WH-8*	CA3	2.20	1.34	3.14	0.36	1.38	0.26	0.07	0.25	0.03	0.19	1.26	0.03	0.09	0.01	0.07	0.01	7.24	1.06	1.60	37.29	1.43	0.94	77.55	1.28	1.25
WH-9*	CA3	2.40	1.21	2.14	0.24	0.94	0.21	0.05	0.23	0.03	0.23	1.61	0.05	0.15	0.02	0.14	0.02	5.66	1.05	1.16	34.26	1.32	1.45	19.84	0.59	1.06
WH-10	CA3	**2.90**	**0.98**	**1.46**	**0.19**	**0.77**	**0.17**	**0.04**	**0.19**	**0.03**	**0.21**	**1.69**	**0.04**	**0.15**	**0.02**	**0.14**	**0.02**	**4.41**	**0.93**	**1.15**	**37.74**	**1.45**	**1.63**	**37.78**	**0.48**	**0.98**
WH-11*	CA3	3.20	0.75	1.27	0.13	0.48	0.09	0.02	0.09	0.01	0.10	0.70	0.02	0.06	0.01	0.06	0.01	3.11	1.12	1.16	35.48	1.36	1.39	30.89	0.87	0.93
WH-12*	CA3	3.50	6.78	13.9	1.50	5.60	1.04	0.23	1.01	0.14	0.81	5.71	0.15	0.42	0.05	0.31	0.04	31.99	1.09	1.26	37.95	1.46	1.01	2.59	1.50	1.17
WH-13	CA3	**3.80**	**0.91**	**1.43**	**0.17**	**0.69**	**0.14**	**0.03**	**0.17**	**0.03**	**0.18**	**1.52**	**0.04**	**0.13**	**0.02**	**0.12**	**0.02**	**4.09**	**1.04**	**1.21**	**38.04**	**1.46**	**1.64**	**37.08**	**0.50**	**0.98**
WH-14	CA3	**4.20**	**3.13**	**5.13**	**0.67**	**2.69**	**0.62**	**0.16**	**0.73**	**0.12**	**0.81**	**6.43**	**0.17**	**0.53**	**0.07**	**0.42**	**0.06**	**15.29**	**0.97**	**1.25**	**37.8**	**1.45**	**1.70**	**12.3**	**0.5**	**1.12**
WH-15*	CA3	4.40	13.91	22.53	1.90	7.39	1.43	0.42	1.79	0.27	1.83	17.92	0.40	1.25	0.16	0.93	0.12	54.32	1.44	1.46	45.03	1.73	1.65	83.43	1.01	1.00
WH-16	CA3	**4.60**	**6.07**	**9.43**	**0.86**	**3.46**	**0.67**	**0.19**	**0.83**	**0.12**	**0.80**	**7.69**	**0.17**	**0.52**	**0.07**	**0.38**	**0.05**	**23.62**	**1.37**	**1.47**	**44.51**	**1.71**	**1.55**	**32.32**	**1.09**	**1.05**
WH-17*	CA3	4.80	2.23	4.24	0.57	2.29	0.47	0.11	0.43	0.06	0.32	1.88	0.06	0.15	0.02	0.11	0.02	11.08	0.93	1.38	33.86	1.30	0.88	6.81	1.31	1.34